Functional Mapping of Yeast Genomes by Saturated Transposition

Agnès H. Michel[1], Riko Hatakeyama[2], Philipp Kimmig[1], Meret Arter[1], Matthias Peter[1], Joao Matos[1], Claudio De Virgilio[2] and Benoît Kornmann[1]*

[1]Institute of Biochemistry
ETH Zurich
8093 Zürich – Switzerland

[2]Department of Biology
University of Fribourg
1700 Fribourg – Switzerland.

*Correspondence to benoit.kornmann@bc.biol.ethz.ch

Yeast is a powerful model for systems genetics. We present a versatile, time- and labor-efficient method to functionally explore the *Saccharomyces cerevisiae* genome using saturated transposon mutagenesis coupled to high-throughput sequencing. SAturated Transposon Analysis in Yeast (SATAY) allows one-step mapping of all genetic loci in which transposons can insert without disrupting essential functions. SATAY is particularly suited to discover loci important for growth under various conditions. SATAY (1) reveals positive and negative genetic interactions in single and multiple mutant strains, (2) can identify drug targets, (3) detects not only essential genes, but also essential protein domains, (4) generates both null and other informative alleles. In a SATAY screen for rapamycin-resistant mutants, we identify Pib2 (PhosphoInositide-Binding 2) as a master regulator of TORC1. We describe two antagonistic TORC1-activating and -inhibiting activities located

30   **on opposite ends of Pib2. Thus, SATAY allows to easily explore the yeast genome at**

31   **unprecedented resolution and throughput.**

32

Introduction

33

34   *Saccharomyces cerevisiae* is an invaluable model for cell biology (Weissman, 2010). Despite the

35   simplicity of its genome, its inner working mechanisms are similar to that of higher eukaryotes.

36   Furthermore, its ease of handling allows large-scale screenings. Yeast genetic screens have classically

37   been performed by random mutagenesis, followed by a selection process that identifies interesting

38   mutants. However elegant the "tricks" implemented to expose the sought-after mutants, this

39   selection phase remains a tedious process of finding a needle-in-a-haystack (Weissman, 2010). The

40   selection phase can limit the throughput and the saturation of classical yeast genetic screens.

41   To circumvent these problems, a second-generation genetic screening procedure has been developed.

42   Ordered deletion libraries for every non-essential gene have been generated (Giaever et al., 2002).

43   The growth of each individual deletion strain can be assessed, either by robot-mediated arraying, or

44   by competitive growth of pooled deletion strains, followed by detection of "barcodes" that identify

45   each deletion strain. These second-generation approaches also have limitations. First, ordered

46   libraries of complete deletions only cover non-essential genes. Second, deletion strains are prone to

47   accumulate suppressor mutations (Teng et al., 2013). To alleviate these problems, deletion libraries

48   can be propagated in a diploid-heterozygous form. Additional steps are then required to make them

49   haploid. In addition, while single genetic traits can be crossed into a pre-existing library, allowing for

50   instance pairwise genetic-interaction analysis (Costanzo et al., 2010), introducing multiple and/or

51   sophisticated genetic perturbations becomes problematic, since crossing requires a selection marker

52   for each important trait. Typically, deletion libraries are missing in most biotechnology-relevant

53 backgrounds. Finally, manipulating ordered libraries requires non-standard equipment, such as

54 arraying robots, limiting the pervasiveness of these approaches.

55 Recently, an innovative approach called Transposon sequencing (Tn-seq) was developed in several

56 bacterial models, and allows *en masse* analysis of a pool of transposon mutants using next-generation

57 sequencing (Christen et al., 2011; Girgis et al., 2007; van Opijnen et al., 2009). This approach

58 alleviates the limitations of previous genetic screens, but is restricted to prokaryotes.

59 Here, we describe an adaptation of the Tn-seq strategy for eukaryotic genomes, that combines the

60 advantages of both first and second generation screens, while alleviating their limitations. The

61 method is based on the generation of libraries of millions of different clones by random transposon

62 insertion (Figure 1A). Transposons inserted in genes that are important for growth kill their hosts and

63 are not subsequently detected. These genes therefore constitute transposon-free areas on the

64 genomic map. Transposon-based libraries can be grown in any condition to reveal condition-specific

65 genetic requirements. Unlike ordered deletion libraries, transposon-based libraries can easily be

66 generated *de novo* from different strain backgrounds, are not limited to coding sequences and do not

67 require the usage of robots.

68 This method can successfully uncover sets of genes essential in given conditions, genome-wide

69 genetic interactions and drug-targets. Transposon insertions can generate loss- and gain-of-function

70 variants. Finally, our approach not only shows which protein is important for growth, but also which

71 part of the protein is essential for function, allowing genome-wide mapping of structural protein

72 domains and screening of phenotypes at a sub-gene resolution.

73 # Results

74 ## Library generation

75	The detailed procedure can be found in the Methods section. The method utilizes the Maize Ac/Ds
76	transposase /transposon system in yeast (Lazarow et al., 2012; Weil and Kunze, 2000). Briefly, cells in
77	which the *ADE2* gene is interrupted by the MiniDs transposon are induced to express the transposase
78	Ac, on galactose-containing adenine-lacking synthetic defined medium (SD +galactose -adenine).
79	Transposase-induced MiniDs excision is followed by repair of the *ADE2* gene. Cells with repaired *ADE2*
80	will be able to form colonies. The excised transposon then re-inserts at random genomic locations
81	with a frequency of ~60% (Lazarow et al., 2012).
82	We have generated seven libraries, displayed together in all figures to illustrate the reproducibility of
83	the approach. All libraries were generated in *ade2Δ* strains derived from BY4741 and BY4742
84	backgrounds. Additional mutations (*dpl1Δ*, *dpl1Δ psd2Δ*, *VPS13(D716H)*, *mmm1Δ VPS13(D716H)*,
85	*YEN1^{on}*, Table 1) will be described in the following sections. The complete dataset is available
86	(Supplementary File 1) and searchable here:
87	http://genome-euro.ucsc.edu/cgi-
88	bin/hgTracks?hgS_doOtherUser=submit&hgS_otherUserName=benjou&hgS_otherUserSessionNam
89	e=23bDePuYrk

Detection of transposon insertion sites

91	Typically 7,000-10,000 colonies with a narrow size distribution (Figure 1 – figure supplement 1) can
92	be generated on a 8.4 cm-Ø petri dish. In the case of wild-type library 1, 240 plates yielded ~1.6E6
93	clones (Table 1). To detect transposon insertion sites, transposed cells were scraped off the 240 plates
94	and pooled (Figure 1A). This pool was used to reinocculate SD medium lacking adenine (SD +Dextrose
95	-Adenine), and the culture was grown to saturation. This step was used to dilute non-transposed *ade*-
96	cells still present on the petri dishes. The culture was then harvested by centrifugation. Genomic DNA
97	was extracted and digested with frequent-cutting restriction enzymes, followed by ligase-mediated

98   intramolecular circularization. Circular DNA was PCR-amplified using transposon-specific outwards-

99   facing primers. PCR products were then sequenced on a MiSeq machine (Figure 1A).

100   ## Analysis of transposon insertion sites

101   We aligned the sequencing reads of the wild-type library (Table 1) to the reference yeast genome and

102   counted the number of mapped transposons. To account for the fact that Illumina sequencing is

103   imperfectly accurate, we considered that two reads of the same orientation mapping within two bp of

104   each other originated from the same transposon (see MatLab Script 1). In this analysis, 284,162

105   independent transposons could be mapped onto the genome, representing an average density of one

106   transposon every 42 bp, and a median number of 22 reads per transposon. No large area of the

107   genome was devoid of transposon (Figure 1B). Consistent with analyses in Maize (Vollbrecht et al.,

108   2010), no strong sequence preference was detected in the insertion sites (Figure 1 – figure

109   supplement 2A).

110   In many instances, though, insertion frequency was modulated along the genome with a periodicity

111   of ~160 bp. Superimposing nucleosome occupancy data (Lee et al., 2007) showed that this was due

112   to favored transposon insertion in inter-nucleosomal DNA (Figure 1 – figure supplement 2B). This

113   effect can be appreciated at the genome-scale. Indeed, an autocorrelation analysis unraveled a ~160

114   bp periodic signal in the genome-wide transposon density (measured using a 40 bp moving average,

115   Figure 1 – figure supplement 2C). This periodicity was comparable to that of the nucleosomal density

116   data (Lee et al., 2007). Finally, while no large region was devoid of transposon, some regions were

117   actually preferentially targeted by transposons. These were the pericentromeric regions (Figure 1B,

118   top), which were specifically enriched by ~20% of the transposon insertions (Figure 1 – figure

119   supplement 2D). The explanation for this phenomenon may pertain to nuclear architecture and to the

120   propensity of our transposon to insert close to its excision site (Lazarow et al., 2012). Because the

121 transposon is initially excised from a centromeric plasmid, and because centromeres cluster in the

122 nuclear periphery (Jin et al., 2000), the transposon might tend to reinsert in the pericentromeric

123 regions of other chromosomes. We confirmed this assumption by sequencing a small-scale library

124 (~30 000 insertions mapped) in which the MiniDS transposon was originally at the endogenous *ADE2*

125 locus, rather than on a centromeric plasmid. In this library, preferential targeting was not observed at

126 pericentromeric regions, but rather in the vicinity of *ADE2*, confirming our assumption (Figure 1B,

127 bottom).

Identification of essential genes

129 The transposon map clearly showed that a fraction of the coding DNA sequences (CDS) were devoid of

130 insertions. These coincided almost exactly with genes annotated as essential (Figure 1C, green

131 arrowheads). The median number of transposon inserted in the CDSs of all genes was 18 per gene

132 (Figure 1D). This number raised to 21 for annotated non-essential genes, but dropped to 3 for

133 annotated essential genes (Figure 1E). This decrease was not due to a difference in the length

134 between essential and non-essential genes, since normalizing the number of transposon insertions to

135 the CDS length (transposon density) did not abrogate this effect (Figure 1 – figure supplement 3).

136 Thus our method distinguishes, in a single step, genes that are required for growth from those that

137 are not.

138 Several genes, although annotated as non-essential, harbored no or very few transposons

139 (Supplementary File 2). This can be attributed to the following reasons. (1) Because sequencing reads

140 mapping to repeated sequences were discarded during alignment, repeated genes appear as

141 transposon-free. (2) Several annotated dubious ORFs overlap with essential genes, and thus appear as

142 transposon-free. (3) Several genes are necessary for growth in particular conditions, and are therefore

143   not annotated as essential, yet are required in our growth conditions (SD +galactose -adenine). These

144   include genes involved, for instance, in galactose metabolism and adenine biosynthesis.

145   ## Identification of protein domains

146	It came as a surprise that some genes annotated as essential were tolerant to transposon insertion.
147	While some of these clearly corresponded to annotation inconsistencies, many reflected an
148	unanticipated outcome of our approach. We observed many instances of "essential" CDSs containing
149	transposon-permissive regions. A striking example is *GAL10* (Figure 2A). *GAL10* encodes a bifunctional
150	enzyme with an N-terminal epimerase, and a C-terminal mutarotase domain (Majumdar et al., 2004).
151	While the epimerase activity is indispensable in our conditions, the mutarotase activity is dispensable,
152	as cells were fed a mixture of α- and β-D-Galactose, thus not requiring the conversion of one into the
153	other. In accordance, the 3' end of *GAL10* was permissive for transposon insertion. The junction
154	between the permissive and non-permissive domains of *GAL10* corresponds exactly to the junction of
155	the two domains in the Gal10 protein. Several examples of essential genes with dispensable 3'-ends
156	are shown in Figure 2A. We confirmed the dispensability of the 3' end for two genes, *TAF3* and *PRP45*
157	(Figure 3).

158	*TAF3* encodes a 47-kDa central component of TFIID (Sanders et al., 2002). Our data show that only the
159	first 76 amino acids are necessary for growth. Using homologous recombination, we replaced all but
160	the sequence coding for the first 90 amino acids with an HA tag and a G418-resistance cassette
161	(*KanMX6*) in a diploid strain. Sporulation and progeny segregation confirmed that strains expressing
162	only the first 90 amino acids of Taf3 were viable (Figure 3A). By contrast, complete replacement of
163	*TAF3* gave rise to only two viable, G418-sensitive spores per meiosis, confirming that *TAF3* is essential
164	(Figure 3B). The essential region of Taf3 corresponds to a predicted histone-like bromo-associated
165	domain (Doerks et al., 2002).

166	*PRP45* encodes a central component of the spliceosome. From our data, only the first 140 amino-acids
167	of Prp45 are necessary for growth, which we confirmed using the same strategy as for *TAF3* (Figure
168	3C-D). Prp45 is predicted to be intrinsically disordered, thus no clear domain boundaries are available
169	to rationalize our data. However, a recent cryo-EM structure of the *S. cerevisiae* spliceosome offers

170	clues on the structure of Prp45 (Wan et al., 2016). Prp45 is centrally located within the spliceosome,
171	has an extended conformation and makes several contacts with various proteins and snRNAs. In
172	particular, the most conserved region of Prp45 is a loop that makes extensive contacts with U2 and U6
173	snRNAs close to the active site (Figure 3E-F, yellow). This loop belongs to the dispensable part of
174	Prp45, surprisingly suggesting that splicing can occur without it. Our method thus offers insights that
175	neither sequence conservation nor structural analysis could have predicted.
176	We also observed CDSs in which the 5' end is permissive for transposon insertion while the 3' end is
177	not (Figure 2B-C). Again, our data show a general good coincidence between indispensable regions
178	and annotated domains. It is surprising that transposons can be tolerated in the 5' of such genes,
179	since several stop codons in all frames of the transposon should interrupt translation and prevent the
180	production of the essential C-terminus. We speculate that the production of the C-terminus is enabled
181	by spurious transcription events. A remarkable example is *SEC9* (Figure 2C). *SEC9* encodes a SNARE
182	protein. The essential SNARE domain, located at the C-terminus (Brennwald et al., 1994), is devoid of
183	transposons. The N-terminus of the protein is known to be dispensable for growth (Brennwald et al.,
184	1994). We indeed observe several transposons inserted upstream of the SNARE domain. The extreme
185	5' of the gene constitutes another transposon-free region even though it encodes a dispensable part
186	of the protein (Brennwald et al., 1994). It is possible that transposon insertion in this 5' region
187	generates an unexpressed, unstable or toxic protein. Other examples of genes showing various
188	combinations of essential domains are shown in Figure 2C.
189	We devised an algorithm to score genes according to their likelihood of bearing transposon-tolerant
190	and -intolerant regions (MatLab Script 2). In short, we computed for each CDS the longest interval
191	between five adjacent transposons, multiplied it by the total number of transposons mapping in this
192	CDS, and divided the result by the CDS length. We additionally imposed the following criteria: the
193	interval must be at least 300 bp, must represent more than 10% and less than 90% of the CDS length,

194　　　and a minimum of 20 transposons must map anywhere within the CDS. ~1200 genes fulfilled these

195　　　requirements (Figure 2 – figure supplement 1), of which the 400 best-scoring ones showed clear

196　　　domain boundaries (Figure 2 – figure supplement 2-5). Essential subdomains are only expected in

197　　　essential genes and indeed, this gene set was overwhelmingly enriched for previously-annotated

198　　　essential genes (Figure 2 – figure supplement 1).

199　　　Thus, our method allows to identify not only genes, but also subdomains that are important for

200　　　growth, yielding valuable structure-function information about their cognate proteins.

Comparison of independent libraries reveals genetic interactions

201

202　　　Our approach can easily identify essential genes and essential protein domains. In addition, its ease

203　　　makes it a potential tool to uncover genes that are not essential in standard conditions but become

204　　　important in specific conditions. Indeed, our approach yields two measures — the number of

205　　　transposons mapping to a given gene, and the corresponding numbers of sequencing reads. Since in

206　　　most cases, transposon insertion obliterates the gene function, both measures may be used as a proxy

207　　　for fitness. We assessed the usefulness of these metrics in various genetics screens.

208　　　Synthetic genetic interaction screening is an extremely powerful approach to establish networks of

209　　　functional connections between genes and biological pathways, and to discover new protein

210　　　complexes (Costanzo et al., 2010; Schuldiner et al., 2005). We have recently identified single amino-

211　　　acid substitutions in the endosomal protein Vps13 that suppress the growth defect of mutants of the

212　　　ER-mitochondria encounter structure (ERMES) (Lang et al., 2015b). Suppression is dependent on the

213　　　proper function of the mitochondrial protein Mcp1 (Tan et al., 2013) and on the endosomal protein

214　　　Vam6/Vps39 (Elbaz-Alon et al., 2014; Hönscher et al., 2014). We generated a transposon library from

215　　　a strain bearing both the *VPS13* suppressor allele *VPS13(D716H)* and a deletion of the ERMES

216　　　component *MMM1*. In these conditions, we expected *VPS13*, *MCP1* and *VAM6/VPS39* to become

217	indispensable, while ERMES components (*MDM10*, *MDM12* and *MDM34*) should become dispensable.
218	Figure 4A shows, for each of the 6603 yeast CDSs, the number of transposon insertion sites mapped in
219	the wild-type (x-axis) and in the *mmm1Δ VPS13(D716H)* library (y-axis). Most CDSs fall on a diagonal,
220	meaning that they were equally transposon-tolerant in both libraries. Consistent with the ERMES
221	suppressor phenotype of the *VPS13(D716H)* mutation, ERMES components fell above the diagonal
222	(that is, they bore more transposons in the *mmm1Δ VPS13(D716H)* than in the wild-type library,
223	Figure 4A-B). By contrast, *VPS13*, *MCP1* and *VAM6/VPS39* fell under the diagonal, as expected (Lang
224	et al., 2015, Figure 4A, C). Many other genes known to display synthetic sick or lethal interaction with
225	*mmm1Δ* (Hoppins et al., 2011) were also found, including *TOM70, VPS41, YPT7, VMS1* and *YME1*
226	(Figure 4A, C).
227	As a second proof-of-principle, we generated a library from a strain in which the dihydrosphingosine
228	phosphate lyase gene *DPL1* (Saba et al., 1997) was deleted, and another library from a strain in which
229	both *DPL1* and the phosphatidylserine decarboxylase 2 gene *PSD2* (Trotter and Voelker, 1995) were
230	deleted (Figure 4D, F). In this latter double-deleted strain, phosphatidylethanolamine can only be
231	generated via the mitochondrial phosphatidylserine decarboxylase Psd1, and thus any gene required
232	for lipid shuttling to and from mitochondria should become indispensable (Birner et al., 2001).
233	*LCB3*, which displays synthetic sick interaction with *DPL1* (Zhang et al., 2001), was less transposon-
234	tolerant in both the *dpl1Δ* and the *dpl1Δ psd2Δ* libraries (Figure 4D). By contrast *PSD1*, which displays
235	a synthetic lethality with *PSD2* on media lacking choline and ethanolamine (Birner et al., 2001), was
236	transposon-intolerant in the *dpl1Δ psd2Δ* library only (Figure 4F-G). Interestingly, we also found that
237	*VPS13* was less transposon-tolerant in the *dpl1Δ psd2Δ*, consistent with a role for Vps13 in
238	interorganelle lipid exchange (AhYoung et al., 2015; Kornmann et al., 2009; Lang et al., 2015a,
239	2015b).

240   Additionally, when comparing the *dpl1Δ* and wild-type libraries, one of the best hits was the histidine

241   permease *HIP1* (Figure 4D-E). This did not, however, reflect a genetic interaction between *HIP1* and

242   *DPL1*, but instead between *HIP1* and *HIS3*; during the construction of the strains, *ADE2* was replaced

243   by a *HIS3* cassette in the wild-type strain, while it was replaced by a NAT cassette in the *dpl1Δ* strain.

244   The histidine-auxotroph *dpl1Δ* strain, therefore required the Hip1 permease to import histidine.

245   Thus, synthetic genetic interactions are visible through pairwise comparison of the number of

246   transposons per genes. However, this metrics leads to a significant spread of the diagonal (Figure 4A,

247   D, F). This spread is due to the intrinsic noise of the experiment. Indeed, the number of transposons

248   per gene is expected, for each gene, to follow a binomial distribution. Sampling variability may thus

249   mask biologically relevant differences. To overcome this limitation, we reasoned that comparing sets

250   of one or more libraries against each other, rather than comparing two libraries in a pairwise fashion

251   (as in Figure 4), would greatly improve the signal-to-noise ratio. We thus calculated an average fold-

252   change of the number of transposons per gene between the experimental and reference sets, as well

253   as a *p*-value (based on a Student's t-test) associated with this change. The fold-change and *p*-values

254   were then plotted as a volcano plot (Figure 4 – figure supplement 1, Supplementary File 3). In volcano

255   plots, synthetic genes appeared well separated from the bulk of neutral genes, showing that parallel

256   library comparison is a robust way to increase the signal-to-noise ratio.

257   Synthetic lethality is one type of genetic interaction. Another type is rescue of lethal phenotype,

258   where a gene deletion is lethal in an otherwise wild-type strain but can be rescued by a suppressor

259   mutation. We describe two such phenomena observed in our libraries. The first concerns the septin

260   gene *CDC10*. Septin proteins are cytoskeletal GTPases that form a ring at the bud neck. This structure

261   is necessary for vegetative growth in *S. cerevisiae*, and all septin genes are essential with the

262   exception of *CDC10* (Bertin et al., 2008; McMurray et al., 2011). Indeed, at low temperature, *cdc10Δ*

263   cells are viable and able to assemble a septin ring. This Cdc10-less ring is based on a Cdc3-Cdc3

264	interaction, instead of the normal Cdc3-Cdc10 interaction (McMurray et al., 2011). Because the
265	propensity of Cdc3 to self-assemble is weak, low temperature is thought to be necessary to stabilize
266	the interaction. Since we grew all libraries at moderately high temperature (30˚C), *CDC10* was, as
267	expected, essentially transposon-free in most libraries (Figure 5A). In the *dpl1Δ psd2Δ* library,
268	however, the number of transposons mapping within *CDC10* increased significantly, indicating that
269	the absence of Psd2 and Dpl1 suppressed the *cdc10Δ* phenotype (Figure 5A, Figure 4 – figure
270	supplement 1, bottom left). Genetic analysis revealed that the *dpl1Δ* allele alone allowed *cdc10Δ* cells
271	to grow at higher temperature, indicating that the Cdc10-less septin ring was stabilized in the
272	absence of Dpl1 (Figure 5B-C). Genetic analysis also demonstrated that the rescue of *cdc10Δ* by *dpl1Δ*
273	was independent of *PSD2*. It is unclear why the suppressive effect was detected in the *dpl1Δ psd2Δ*
274	library, but not in the *dpl1Δ* library. We speculate that differences in growth conditions between
275	experiments have obscured either the suppression in the *dpl1Δ* library or the involvement of Psd2 in
276	our tetrad analyses.
277	Dpl1 is an ER protein that does not contact any of the septin subunits; its destabilizing effect on the
278	septin ring must therefore be indirect. Since Dpl1 is a regulator of sphingolipid precursors (Saba et al.,
279	1997) and since the septin ring assembles in contact with the plasma membrane (Bertin et al., 2010),
280	it is most likely the changing properties of the membrane in *DPL1*-deficient cells that allow or restrict
281	the assembly of Cdc10-less septin rings. This hypothesis is particularly appealing because
282	temperature has a profound effect on membrane fluidity and composition (Ernst et al., 2016). Thus,
283	the stabilizing effect of low temperature on Cdc10-less septin rings might not only be the result of a
284	direct stabilization of Cdc3-Cdc3 interaction, but also of changes in plasma membrane properties,
285	which can be mimicked by *DPL1* ablation.
286	The second example of rescue of a lethal phenotype was observed in a library made from a strain
287	expressing a constitutively active version of the Holliday-junction resolvase Yen1, a member of the

288	Xeroderma Pigmentosum G (XPG) family of 5'-flap endonucleases (Ip et al., 2008). In wild-type
289	strains, Yen1 is kept inactive during the S-phase of the cell cycle via Cdk-mediated phosphorylation
290	(Matos et al., 2011). Rapid dephosphorylation at anaphase activates Yen1 for the last stages of
291	mitosis. When nine Cdk1 target sites are mutated to alanine, Yen1 becomes refractory to inhibitory
292	phosphorylation and active during S-phase (Yen1^{on}) (Blanco et al., 2014). To investigate the cellular
293	consequence of a constitutively active Yen1, we generated a library in a *YEN1^{on}* background. We
294	discovered that, under these conditions, the essential gene *DNA2* became tolerant to transposon
295	insertion (Figure 5D). Further genetic analyses confirmed that the presence of the *YEN1^{on}* allele led to
296	a rescue of the lethal phenotype of *dna2Δ* strains; spores bearing the *dna2* deletion failed to grow
297	unless they additionally bore the *YEN1^{on}* allele (Figure 5E). Moreover, at 25°C, the colony size of
298	*dna2Δ YEN1^{on}* spores was comparable to that of the *DNA2* counterparts (Figure 5E, right). However,
299	FACS analysis of DNA content revealed that *dna2Δ YEN1^{on}* cells accumulated in S- and G2-phases
300	(Figure 5F).
301	*DNA2* encodes a large protein with both helicase and endonuclease activities (Budd and Campbell,
302	1995). Interestingly, while the helicase activity can be disrupted without affecting yeast viability, the
303	nuclease activity is essential (Ölmezer et al., 2016), presumably due to its involvement in processing
304	long 5'-flaps of Okazaki fragments. Our genetic data now reveal that Yen1 is able to partially fulfill the
305	essential roles of *DNA2*, provided that its activity is unrestrained in S-phase. Since the spectrum of
306	Yen1 substrates includes 5'-flap structures (Ip et al., 2008), Yen1^{on} may be able to substitute the
307	essential function of Dna2 by providing 5'-flap nuclease activity in S-phase. This finding extends
308	previous work showing that Yen1 serves as a backup for the resolution of replication intermediates
309	that arise in helicase-defective mutants of DNA2 (Ölmezer et al., 2016).
310	Thus, our method can be used to screen for negative and positive genetic interactions in a rapid,

14

311   labor-efficient and genome-wide manner, in strains bearing single and multiple mutations

Chemical Genetics Approach

313   To assess our method's ability to uncover drug targets, we used the well-characterized immune-

314   suppressive macrolide rapamycin. Rapamycin blocks cell proliferation by inhibiting the target of

315   rapamycin complex I (TORC1), through binding to the Fk506-sensitive Proline Rotamase Fpr1

316   (Heitman et al., 1991). The TORC1 complex integrates nutrient-sensing pathways and regulates

317   cellular growth accordingly. Rapamycin treatment therefore elicits a starvation response, which stops

318   proliferation. We generated and harvested a wild-type library, then grew it in medium containing

319   rapamycin at low concentration. To compare it to an untreated wild-type library, we counted the

320   number of sequencing reads mapping to each of the 6603 yeast CDSs in both conditions (Figure 6A).

321   Most genes fell on a diagonal, as they do not influence growth on rapamycin. By contrast, a few genes

322   were robustly covered by sequencing reads in the rapamycin-treated library, indicating that their

323   interruption conferred rapamycin resistance. Expectedly, the best hit was *FPR1*, encoding the receptor

324   for rapamycin (Hall, 1996). Other hits included *RRD1* (Rapamycin-Resistant Deletion 1), *TIP41*, *GLN3*,

325   *SAP190*, *PSP2*, *CCS1*, *ESL2* and members of the PP2A phosphatase *PPH21* and *PPM1* (Figure 6A). These

326   genes are either directly involved in rapamycin signaling or known to confer rapamycin resistance

327   upon deletion (Xie et al., 2005).

328   Finding the TORC1 regulator *PIB2* (Kim and Cunningham, 2015) was however unexpected, because

329   *PIB2* deletion confers sensitivity, not resistance, to rapamycin (Kim and Cunningham, 2015; Parsons et

330   al., 2004). To solve this conundrum, we looked at the distribution of transposons on the *PIB2* coding

331   sequence. All the insertions selected by rapamycin treatment mapped to the 5'-end of the gene

332   (Figure 6B). On the contrary, the rest of *PIB2* was less covered in the rapamycin-treated than in non-

333   rapamycin-treated libraries (Figure 6 – figure supplement 1A). Insertions in the 5' end of *PIB2*

334   therefore conferred rapamycin resistance, while insertions elsewhere, like complete deletion of *PIB2*,

335   conferred rapamycin sensitivity.

336   To confirm this result, we engineered N-terminal truncations of Pib2, guided by the transposon map.

337   Strains expressing Pib2 variants that were truncated from the first until up to amino acid 304 were

338   hyperresistant to rapamycin (Figure 6C, top). We also confirmed that, by contrast, complete *PIB2*

339   deletion caused rapamycin hypersensitivity. A larger N-terminal truncation extending beyond the

340   mapped territory of rapamycin resistance-conferring transposons, did not mediate hyperresistance to

341   rapamycin (Figure 6G, Pib2$^{426\text{-}635}$).

342   To assess whether rapamycin-hyperresistant *PIB2* truncations behaved as gain-of-function alleles,

343   we co-expressed Pib2$^{165\text{-}635}$ and full-length Pib2. In these conditions, the rapamycin hyperresistance

344   was mitigated, indicating that the effect of the truncated Pib2 protein was semi-dominant (Figure 6C,

345   bottom). Expressing the truncation from a high-copy (2µ) vector did not further increase resistance to

346   rapamycin, indicating that higher expression levels did not change the semi-dominance of the *PIB2*

347   truncation allele.

348   Thus, Pib2 truncation leads to a gain-of-function that translates into semi-dominant rapamycin

349   hyperresistance. Because gain-of-function alleles of *PIB2* lead to rapamycin resistance, while loss-of-

350   function alleles lead to sensitivity, our data suggest that Pib2 positively regulates TORC1 function. To

351   test this idea further, we investigated the effects of full-length and various truncations of Pib2 on

352   TORC1 signaling. Switching yeast cells from a poor nitrogen source (proline) to a rich one (glutamine)

353   triggers a fast activation of TORC1 (Stracka et al., 2014), leading to a transient surge in the

354   phosphorylation of Sch9, a key target of TORC1 in yeast (Urban et al., 2007). We cultured cells on

355   proline-containing medium and studied TORC1 activation 2 minutes following addition of 3 mM

356   glutamine by determining the phosphorylation levels of Sch9-Thr^{737}. Pib2 deficiency severely blunted

357   TORC1 activation in these conditions (Figure 6D, top). In a control experiment, a strain lacking *GTR1* –

358	a component of the TORC1-activating EGO (Exit from rapamycin-induced GrOwth arrest) complex,
359	which is orthologous to the mammalian Rag GTPase-Ragulator complex (Chantranupong et al., 2015;
360	Powis and De Virgilio, 2016) – showed a similarly blunted response with respect to TORC1 activation
361	following glutamine addition to proline-grown cells (Figure 6D, top). By contrast, glutamine-
362	mediated TORC1 activation appeared normal in a strain expressing an N-terminally truncated Pib2
363	variant (*pPIB2$^{165-635}$*, Figure 6D, bottom). Thus, like Gtr1, Pib2 is necessary to activate TORC1 in
364	response to amino acids. The N-terminus of Pib2 appears to be an inhibitory domain. The ablation of
365	this domain confers rapamycin resistance, yet is not sufficient to constitutively activate TORC1 (*e.g.* in
366	proline-grown cells).
367	Having identified an inhibitory activity at the N-terminus of Pib2, we proceeded to address the
368	function of other Pib2 domains. To this aim, we used a split-ubiquitin-based yeast-two-hybrid assay
369	to probe the interaction of Pib2 fragments with the TORC1 component Kog1, and studied the
370	rapamycin resistance of strains expressing various truncations of Pib2 (Figures 6E-F). We found that
371	Pib2 harbored at least two central Kog1-binding regions, since two mostly non-overlapping
372	fragments (Pib2$^{1-312}$ and Pib2$^{304-635}$) showed robust interaction with Kog1 (Figure 6F and Figure 6 –
373	figure supplement 1B). Kog1 binding is, however, not essential for Pib2-mediated TORC1 activation,
374	since cells expressing a fragment without these Kog1-binding domains (Pib2$^{426-635}$) were as
375	rapamycin-resistant as cells expressing full length Pib2 (FL, Figure 6G).
376	Pib2 harbors a phosphatidylinositol-3-phosphate (PI3P) -binding Fab1-YOTB-Vac1-EEA1 (FYVE)
377	domain (Figure 6E). Pib2 truncations lacking the FYVE domain are unable to bind PI3P, and hence to
378	properly localize to the vacuole (Kim and Cunningham, 2015). When cells expressed FYVE domain-
379	truncated Pib2 (Pib2$^{\Delta426-532}$), their rapamycin resistance decreased, but not as severely as observed in
380	*pib2Δ* strains (Figure 6G). This indicates that FYVE-domain-mediated vacuolar recruitment is not
381	absolutely required for Pib2 to activate TORC1.

382   Strikingly, cells expressing Pib2 variants that were either truncated at the extreme C-terminus ($PIB2^{1-}$

383   ^{620}) or carried a deletion within the C-terminus ($PIB2^{\Delta533-620}$) were as sensitive to rapamycin as $pib2\Delta$

384   cells (Figure 6G). The C-terminus of Pib2 is therefore important to ensure proper TORC1 activation.

385   We conclude that Pib2 harbors the following functional domains: a large N-terminal Inhibitory

386   Domain (NID), and a C-terminal TORC1-Activating Domain (CAD); the central portion of the protein

387   harbors FYVE and Kog1-binding domains for proper targeting of Pib2 to the vacuole and TORC1,

388   respectively.

389   Could the NID act in an auto-inhibitory allosteric fashion by preventing the CAD from activating

390   TORC1? We reasoned that if this were the case, plasmid-encoded N-terminally truncated Pib2 should

391   confer similar levels of rapamycin resistance independently of whether a genomic wild-type $PIB2$

392   copy was present or not. However, wild-type cells expressing N-terminally truncated Pib2$^{165-635}$ from a

393   centromeric or a multi copy 2μ plasmid were less resistant to rapamycin than $pib2\Delta$ cells expressing

394   Pib2$^{165-635}$ from a centromeric plasmid (Figure 6C). Thus, the NID activity of the endogenously-

395   expressed wild-type Pib2 is able to mitigate the rapamycin resistance conferred by ectopic expression

396   (or overexpression) of the CAD. Therefore, our data suggest that the NID does not auto-inhibit the CAD

397   within Pib2, but rather, that the NID and CAD act independently and antagonistically on TORC1.

398   This latter scenario predicts that, just as expressing NID-truncated Pib2 semi-dominantly activates

399   TORC1 (Figure 6C), expressing CAD-truncated Pib2 should semi-dominantly inhibit it. To test this

400   prediction, we expressed the two CAD truncations Pib2$^{\Delta533-620}$ and Pib2$^{1-620}$ in an otherwise wild-type

401   strain. The resulting strains were significantly more sensitive to rapamycin than their counterparts

402   expressing only full length Pib2 (Figure 6H). Furthermore, when $pib2\Delta$ cells expressed the Pib2 CAD

403   truncation alleles, they became even more sensitive to rapamycin. Therefore, Pib2-NID does not act in

404   an auto-inhibitory manner, but rather inhibits TORC1 independently of the presence of a Pib2-CAD.

405	Since the Rag GTPase Gtr1-Gtr2 module of the EGO complex also mediates amino acid signals to
406	TORC1 (Binda et al., 2009; Dubouloz et al., 2005, see also Figure 6D), we tested the possibility that
407	Pib2-NID inhibits TORC1 by antagonizing Gtr1-Gtr2. This does not appear to be the case; first, the
408	expression of Pib2$\Delta^{533\text{-}620}$ or Pib2$^{1\text{-}620}$ further enhanced the rapamycin sensitivity of *gtr1Δ gtr2Δ* cells
409	(Figure 6 – figure supplement 1C), and second, the Pib2$\Delta^{533\text{-}620}$- or Pib2$^{1\text{-}620}$–mediated rapamycin
410	hypersensitivity was not suppressed by expression of the constitutively active, TORC1-activating
411	Gtr1^{Q65L}-Gtr2^{S23L} module (Binda et al., 2009; Figure 6 – figure supplement 1D). These results suggest
412	that Pib2-NID inhibits TORC1 independently of the EGO complex.

413	In summary, Pib2 is targeted to TORC1 by binding to the vacuolar membrane through its FYVE domain
414	and to Kog1 via its middle portion. Pib2 harbors two antagonistic activities, one activating and the
415	other repressing TORC1. The dose-independent semi-dominant nature of the respective truncations
416	indicate that both repressing and activating activities influence TORC1 independently and do not
417	appear to compete for the same sites on TORC1.

418	We speculate that high-quality amino acids, such as glutamine, balance the antagonistic TORC1-
419	activating and -repressing activities of Pib2 to tune growth rate according to available resources. In
420	this context, it will be interesting to elucidate how the activities of Pib2 and the EGO complex are
421	coordinated to stimulate TORC1 in response to amino acids.

Discussion

| 422 | |

423	Here we present a novel method based on random transposon insertion and next-generation
424	sequencing, to functionally screen the genome of *Saccharomyces cerevisiae*. SAturated Transposon
425	Analysis in Yeast (SATAY) can reveal positive and negative genetic interactions, auxotrophies, drug-
426	sensitive or -resistant mutants, and map functional protein domains. SATAY combines advantages
427	from both classical genetics and high-throughput robotic screens. SATAY can in principle be

428 implemented in any strain background, since it does not rely on the existence of available deletion

429 libraries and does not necessitate markers to follow genetic traits. Moreover, SATAY explores a wide

430 genetic space; exotic alleles can be generated as exemplified by *PIB2* (Figure 6 and Figure 6 – figure

431 supplement 1), where transposon insertions in different regions of the gene generate opposite

432 phenotypes. Transposon insertion is not limited to CDSs; we observe that promoters of essential genes

433 are often transposon-intolerant (Figure 2, see *GAL10, SGV1, MMS21, RET2, HRR25, NPA3, SEC9, SWI1).*

434 We also observe that known essential tRNA, snRNA, as well as SRP RNA genes are transposon

435 intolerant (see Supplementary Dataset). Finally, our data reveal transposon-intolerant areas of the

436 genome that do not correspond to any annotated feature, indicating that SATAY could help discover

437 yet-unknown functional elements.

438 SATAY yields unprecedented insight on the domain structure- function relationship of important

439 proteins, and allows the mapping of important functional domains, without prior knowledge.

440 Dispensable domains in essential proteins might not be required for the essential function of these

441 proteins, but may have other roles. The sub-gene resolution enabled by SATAY may thus unveil yet-

442 unsuspected accessory or regulatory functions, even in otherwise well-studied proteins. In addition,

443 structure-function information revealed by SATAY may guide 3D-structure determination efforts by

444 indicating possibly flexible accessory domains.

445 The resolution of a SATAY screen is directly proportional to the number of transposons mapped onto

446 the genome. The current resolution is ~1/40 bp, which is amply sufficient to confidently identify

447 essential genes and protein domains. This resolution is achieved by mapping ~300,000 transposons,

448 starting from a 1.6E6-colonies library. Not every colony generates a detectable transposon. This is due

449 to several reasons. (1) Excised transposons only reinsert in 60% of the cases (our observations and

450 Lazarow et al., 2012). (2) 7% of the sequencing reads mapped onto repetitive DNA elements (such as

451 rDNA, Ty-elements and subtelomeric repeats) and were discarded because of ambiguous mapping.

452	(3) Two transposons inserted in the same orientation within two bp of each other will be considered
453	as one by our algorithm. This might be exacerbated at densely covered areas of the genome, such as
454	pericentromeric regions. (4) Some transposon insertion products may not be readily amplifiable by
455	our PCR approach.
456	We observe that increasing both the size of the original library and the sequencing depth leads to an
457	increase in mapped transposon number (albeit non-proportional, Table 1). Therefore, the resolution
458	of a screen can be tailored according to the question and the available resource.
459	We could not detect a preferred sequence for transposon insertion (Figure 1 -figure supplement 2A),
460	yet two features of the yeast genome biased insertion frequency in select regions. The first is
461	nucleosome position; the Ac/Ds transposon has a tendency to insert more frequently within inter-
462	nucleosomal regions, indicating that the transposase might have better access to naked DNA (Figure 1
463	-figure supplement 2B-C). The second pertains to a tendency of the transposon to integrate in the
464	spatial proximity of its original location (Lazarow et al., 2012). Indeed, when originated from a
465	centromeric plasmid, the transposon has an increased propensity to reinsert in the pericentromeric
466	regions of other chromosomes. This is not due to a particular feature of pericentromeric chromatin,
467	since this propensity is lost when the transposon original location is on the long arm of ChrXV (Figure
468	1B). Instead, the increased propensity is likely resulting from the clustering of centromeres in the
469	nuclear space (Jin et al., 2000), indicating that centromeric plasmids cluster with the chromosomal
470	centromeres. Thus, SATAY can be utilized to probe, not only the function of the genome, but also its
471	physical and regulatory features, such as nucleosome position and 3D architecture.
472	Finally, SATAY does not require any particular equipment besides access to a sequencing platform,
473	and involves a limited amount of work. It can be easily multiplexed to perform several genome-wide
474	screens simultaneously. Each screen yields two measures, the number of transposons and the number

475	of sequencing reads, both of which, for each gene, reveal the fitness of the cognate mutant. While the
476	number of transposons per gene is appropriate to look for genes that become important for growth,
477	as in genetic interaction screens, the number of sequencing reads is better suited to identify strains
478	that are positively selected, like drug-resistant mutants. Both metrics suffer from intrinsic noise,
479	stemming from the inherently discrete structure of the data, and probably also from unavoidable
480	biases in the amplification and sequencing of the libraries. We show that this noise can be reduced by
481	comparing multiple libraries against each other (Figure 4 – figure supplement 1). Moreover,
482	comparing multiple libraries allows to tailor the composition of each library set to needs. For instance,
483	grouping the *VPS13(D716H)* with the *mmm1Δ VPS13(D716H)* libraries allows to selectively detect
484	synthetic interactions with *VPS13(D716H)* (e.g. ERMES components). By contrast, comparing the
485	*mmm1Δ VPS13(D716H)* library with all others, selectively finds genes important for the ERMES
486	suppression phenomenon. Thus, while signal-to-noise ratio might be a limiting factor for the
487	detection of genetic interactions, we anticipate that increasing the number of libraries, for instance by
488	generating multiple libraries in each conditions, will likely decrease the incidence of false positive and
489	false negative. With the increasing number of screens performed in various conditions will also come
490	the ability to find correlation patterns among genes that are required or dispensable for growth in
491	similar sets of conditions. Such correlations are accurate predictors of common functions and have
492	been extensively used in synthetic genetic screens, such as the E-MAP procedure (Kornmann et al.,
493	2009; Schuldiner et al., 2005). However, while E-MAP screens compute patterns of genetic interaction
494	on a subset of chosen genetic interaction partners, SATAY allows to detect genetic interactions at the
495	genome scale.
496	Because SATAY only necessitates a transposon and a transposase, it should be portable to other
497	industrially-, medically- or scientifically-relevant haploid fungi, such as *S. pombe, Y. lipolytica, C.*
498	*glabrata, K. lactis* and *P. pastoris*.

499	The Ds transposon can in principle accommodate extra sequences with no known length limitation
500	(Lazarow et al., 2013). An interesting future development will be to incorporate functional units in
501	the transposon DNA, for instance strong promoters, repressors or terminators, IRESs, recognition sites
502	for DNA-binding proteins (LacI or TetR), recombination sites (LoxP, FRP), or coding sequences for in-
503	frame fusion, such as GFP, protein- or membrane-binding domains, signal sequences, etc. Improved
504	designs will not only permit finer mapping of protein domains without reliance on spurious
505	transcription and translation, but might allow the exploration of an even wider genetic space, for
506	instance by generating gain-of-function variants, thus enabling the development of novel approaches
507	to interrogate the yeast genome.

Methods

508

Plasmids and strains

509

510

511   All Yeast strains, oligonucleotides and plasmids used herein are listed in Tables 2, 3 and 4,

512 respectively. To generate pBK257, the *ADE2* gene interrupted with the MiniDs transposon was PCR

513 amplified from strain CWY1 (Weil and Kunze, 2000), using PCR primers #4 and #5. The PCR product

514 and pWL80R_4x (plasmid encoding the Ac transposase under the control of the *GAL1* promoter,

515 Lazarow et al., 2012) were digested with SacI, then ligated together. This plasmid does not confer

516 Adenine prototrophy to *ade2Δ* cells unless the Ac transposase excises the MiniDS transposon, and

517 repairs the *ADE2* gene.

518   Deletion strains were generated by PCR-mediated gene replacement using the Longtine toolbox for

519 *KanMX6* and *HIS3* replacement (Longtine et al., 1998) and the Janke toolbox for *NATnt2* (Janke et al.,

520 2004), with primers listed in Table 3. Strain YJM3916 carrying $YEN1^{ON}$ at the endogenous locus was

521 generated using the *delitto perfetto* method (Storici and Resnick, 2003).

Library generation

ade2Δ strains were transformed with the pBK257 plasmid. These strains are phenotypically ade-, since the ADE2 gene borne on the plasmid is interrupted by the MiniDs transposon. One liter of freshly prepared SD -Ura +2% Raffinose + 0.2% Dextrose is inoculated with ade2Δ cells freshly transformed with pBK257, directly scraped off the transformation plates, at a final OD600=0.15. The culture is grown to saturation for 18 to 24hr at 30°C. Cells are spun for 5min at 600x g, 20°C) and resuspended in their supernatant at a final OD600=39. 200 µl of this resuspension are plated on ~250-300 X 8.5cm plates containing 25 ml of SD +2%Galactose -Adenine using glass beads. Plates are incubated in closed but not sealed plastic bags for 3 weeks at 30°C. Clones in which transposon excision has led to the repair of the ADE2 gene on pBK257 start to appear after 10-12 days. The density of clones on the plate reaches 150-200 colonies/cm^2, i.e. 8000-11000 colonies/plates after 3 weeks. All colonies are then scraped off the plates using minimal volume of either water or SD +2% Dextrose -Adenine, pooled, and used to inoculate a 2-liter SD +2% Dextrose -Adenine culture at a density of 2.5 10^6 cells/ml, which is allowed to grow to saturation. This step is used to dilute any remaining ade- cells, which represent about 20% of the total number of cells, and ensures that each transposition event is well represented. For example, reseeding a 2.10^6 clones library in 2L at a density of 2.5 10^6 cells/ml will ensure that each clone is represented by ((2.500.000X1000X2)*0.8)/2.000.000= 2000 cells. The saturated culture is harvested by centrifugation (5 min, 1600x g), washed with ddH2O, then cell pellets are frozen as ~500 mg aliquots.

Rapamycin treatment

Cells scraped off the plates were used to inoculate a 1 liter SD +2% Dextrose -Adenine culture at OD 0.08. After growing for 15 h to OD 0.5, the culture was diluted to OD 0.1 in 500 ml SD +2% Dextrose -Adenine, treated with 10 nM (9.14 ng/ml) rapamycin (Sigma) and grown for 24 h to OD 0.9. The culture was then diluted again to OD 0.1 in 500 ml SD +2% Dextrose -Adenine +10 nM rapamycin.

546   The treated culture was grown to saturation (OD 1.9), harvested by centrifugation and processed for

547   genomic DNA extraction.

548   ## Genomic DNA

549   A 500-mg cell pellet is resuspended with 500 µl Cell Breaking Buffer (2% Triton X-100, 1% SDS, 100

550   mM NaCl, 100 mM Tris-HCl pH8.0, 1 mM EDTA) and distributed in 280µl aliquots. 200 µl

551   Phenol:Chloroform:Isoamylalcool 25:25:1 and 300 µl 0.4-0.6mm unwashed glass beads are added to

552   each aliquot. Samples are vortexed for 10 min at 4℃ using a Disruptor Genie from Scientific Industrial

553   (US Patent 5,707,861). 200 µl TE are added to each lysate, which are then centrifuged for 5 min at

554   16100x g, 4℃. The upper layer (~400 µl) is transferred to a fresh tube, 2.5vol 100% EtOH are added

555   and the sample mixed by inversion. DNA is pelleted for 5 min at 16100x g, 20℃. The supernatant is

556   removed and the pellets resuspended in 200 µl RNAse A 250 µg/ml for 15 min at 55℃, 1000 rpm on a

557   Thermomixer comfort (Eppendorf). 2.5 vol 100% EtOH and 0.1vol NaOAc 3 M pH5.2 are added and the

558   samples mixed by inversion. DNA is pelleted by centrifugation for 5 min at 16100x g, 20℃. The pellets

559   are washed with 70% EtOH under the same conditions, the supernatant removed completely, and the

560   pellets dried for 10 min at 37℃. The pellets are resuspended in a total volume of 100 µl water for 10

561   min at 55℃, 700 rpm on a Thermomixer comfort (Eppendorf).

562   DNA is run on a 0.6% 1X TBE agarose gel against a standard 1 kb GeneRuler, and quantified using FiJi.

563   500 mg cell pellet should yield 20-60 µg DNA.

564   ## Library Sequencing

565   Sequencing involves the following steps: (1) Digestion of genomic DNA with two four-cutter

566   restriction enzymes, (2) ligase-mediated circularization of the DNA, (3) PCR of the transposon-

567   genome junctions using outward-facing primers. (4) Illumina-sequencing of the combined PCR

568   products.

569	2x 2 µg of genomic DNA are digested in parallel in Non-Stick microfuge tubes (Ambion AM12450)
570	with 50 units of DpnII (NEB #R0543L) and NlaIII (NEB #R0125L), in 50 µl for 16 hours at 37℃. The
571	reactions are then heat inactivated at 65℃ for 20 min and circularized in the same tube by ligation
572	with 25 Weiss units T4 Ligase (Thermo Scientific #EL0011) for 6 hours at 22℃, in a volume of 400µl.
573	DNA is precipitated overnight or longer at -20℃ in 0.3 M NaOAc pH5.2, 1 ml 100% EtOH, using 5 µg
574	linear acrylamide (Ambion AM9520) as a carrier, then centrifuged for 20 min at 16100x g, 4℃. Pellets
575	are washed with 1 ml 70% EtOH, for 20 min at 16100 x g, 20℃. After complete removal of the
576	supernatant, pellets are dried for 10 min at 37℃. Each circularized DNA preparation is then
577	resuspended in water and divided into 10X 100 µl PCR reactions. Each 100 µl PCR reaction contains: 10
578	µl 10X Taq Buffer (500 mM Tris-HCl pH9.2, 22.5 mM MgCl2, 160 mM NH4SO4, 20% DMSO, 1% Triton
579	X-100 – stored at -20℃), 200 µM dNTPs, 1 µM primer #1, 1 µM primer #2 , 2.4 µl homemade Taq
580	polymerase. PCR are performed in an MJ Research Peltier Thermal Cycler PTC-200 using the following
581	conditions:
582	Block: calculated – 95℃ 1 min, 35X [95℃ 30 sec, 55℃ 30 sec, 72℃ 3 min], 72℃ 10 min.
583	The 2X 10 PCR reactions are pooled into one NlaIII-digested pool and one DpnII-digested pool. 100µl
584	from each pool are purified using a PCR clean-up/gel extraction kit (Macherey-Nagel) according to the
585	manufacturer protocol, with the following modifications. DNA is bound to the column for 30s at
586	3000x g; 30 µl of elution buffer (10 mM Tris-HCl pH8.5, 0.1% Tween) is applied to the column and
587	incubated for 3 min, then spun for 1 min at 11000x g at 20℃. The eluate is reapplied to the column
588	and a second elution is performed under the same conditions. Purified PCR products are quantified by
589	absorbance at 260 nm. On a 1% agarose gel, the product runs as a smear from 250 bp to 1.2 kb, with
590	highest density centered around 500 bp. The 867 bp size band present in the NlaIII treated sample
591	and the 465 bp size band present in the DpnII treated sample correspond to untransposed pBK257.
592	Equal amounts of DpnII- and NlaIII-digested DNA are pooled and sequenced using MiSeq v3

| 593 | chemistry, according to manufacturer, adding 3.4 µl of 100 µM primer #3 into well 12 of the |
| 594 | sequencing cartridge. |

Bioinformatics Analyses

596	The fastq file generated is uploaded into the CLC genomics workbench, trimmed using adaptor
597	sequences 'GATC' and 'TAGC' (the recognition sites for NlaIII and DpnII, respectively), allowing 2
598	ambiguities and a quality limit of 0.05. The trimmed sequence is then aligned to the reference
599	genome, using the following parameters (mismatch cost, 2; Insertion and deletion costs, 3; length
600	fraction, 1; similarity fraction, 0.95; non-specific match handling, ignore). The alignment is then
601	exported as a BAM file, which is further processed in MatLab, using the MatLab Script 1, to detect
602	individual transposition events. The outputted bed file is uploaded to the UCSC genome browser.
603	Yeast annotations were downloaded from the Saccharomyces Genome Database (SGD). To generate
604	our list of essential genes, we used YeastMine and searched the SGD for genes for which the null
605	mutant has an "inviable" phenotype (Balakrishnan et al., 2012).

606	Volcano plots were computed as follows using MatLab Script 3. Two sets of libraries were defined. For
607	each gene and each library, the number of transposons per gene (tnpergene variable) was normalized
608	to the total number of transposon mapped in the library. For each gene, the fold-change is calculated
609	as the mean of the normalized number of transposons per gene in the experimental set, divided by
610	that in the reference set. The p-value is computed using the Student's t-test by comparing, for each
611	gene, the normalized number of transposons per gene for each library in the experimental and
612	reference sets.

Western blotting

| 614 | Cells were grown to mid-log phase in synthetic minimal medium containing 0.5 g/L proline as a sole |
| 615 | nitrogen source and stimulated with 3 mM glutamine for 2 minutes. Cells were treated with 6.7% |

616   w/v trichloroacetic acid (final concentration), pelleted, washed with 70% ethanol and then lyzed in

617   urea buffer (50 mM Tris-HCl [pH 7.5], 5 mM EDTA, 6 M urea, 1% SDS, 0.1 mg/ml

618   Pefabloc/phosphatase inhibitor mix). After disrupting cells with glass beads and incubating with

619   Laemmli SDS sample buffer, samples were subjected to regular SDS-PAGE and immunoblotting. The

620   phosphorylation level of Sch9-Thr[737] and the total amount of Sch9 were assessed using the

621   phosphospecific anti-Sch9-pThr[737] and anti-Sch9 antibodies, respectively (Péli-Gulli et al., 2015).

622 Split-ubiquitin yeast two-hybrid assay

623   The split-ubiquitin yeast two-hybrid system from Dualsystems Biotech AG was used following the

624   manufacturer's instructions.

625   Pib2 fragments (full-length or truncated) and full-length Kog1 were cloned into pCabWT and pPR3N

626   plasmids, respectively, and transformed into the strain NMY51 as indicated. Protein-protein

627   interactions were detected as growth of the resultant strains on agar plates lacking adenine.

628 Accession Numbers

629   Sequencing data have been deposited at EMBL-EBI ArrayExpress: E-MTAB-4885.

630 Acknowledgements

639 References

640 AhYoung, A.P., Jiang, J., Zhang, J., Khoi Dang, X., Loo, J. a., Zhou, Z.H., and Egea, P.F. (2015). Conserved SMP domains of the ERMES complex
641 bind phospholipids and mediate tether assembly. Proc. Natl. Acad. Sci. 201422363.

642 Balakrishnan, R., Park, J., Karra, K., Hitz, B.C., Binkley, G., Hong, E.L., Sullivan, J., Micklem, G., and Cherry, J.M. (2012). YeastMine--an
643 integrated data warehouse for Saccharomyces cerevisiae data as a multipurpose tool-kit. Database (Oxford). *2012*, bar062.

644 Bertin, A., McMurray, M.A., Grob, P., Park, S.-S., Garcia, G., Patanwala, I., Ng, H.-L., Alber, T., Thorner, J., and Nogales, E. (2008).
645 Saccharomyces cerevisiae septins: supramolecular organization of heterooligomers and the mechanism of filament assembly. Proc. Natl.
646 Acad. Sci. U. S. A. *105*, 8274–8279.

647 Bertin, A., McMurray, M.A., Thai, L., Garcia, G., Votin, V., Grob, P., Allyn, T., Thorner, J., and Nogales, E. (2010). Phosphatidylinositol-4,5-
648 bisphosphate promotes budding yeast septin filament assembly and organization. J. Mol. Biol. *404*, 711–731.

649 Binda, M., Péli-Gulli, M.-P., Bonfils, G., Panchaud, N., Urban, J., Sturgill, T.W., Loewith, R., and De Virgilio, C. (2009). The Vam6 GEF Controls
650 TORC1 by Activating the EGO Complex. Mol. Cell *35*, 563–573.

651 Birner, R., Bürgermeister, M., Schneiter, R., and Daum, G. (2001). Roles of phosphatidylethanolamine and of its several biosynthetic
652 pathways in Saccharomyces cerevisiae. Mol. Biol. Cell *12*, 997–1007.

653 Blanco, M.G., Matos, J., and West, S.C. (2014). Dual Control of Yen1 Nuclease Activity and Cellular Localization by Cdk and Cdc14 Prevents
654 Genome Instability. Mol. Cell *54*, 94–106.

655 Brennwald, P., Kearns, B., Champion, K., Keränen, S., Bankaitis, V., and Novick, P. (1994). Sec9 is a SNAP-25-like component of a yeast
656 SNARE complex that may be the effector of Sec4 function in exocytosis. Cell *79*, 245–258.

657 Budd, M.E., and Campbell, J.L. (1995). A yeast gene required for DNA replication encodes a protein with homology to DNA helicases. Proc.
658 Natl. Acad. Sci. U. S. A. *92*, 7642–7646.

659 Chantranupong, L., Wolfson, R.L., and Sabatini, D.M. (2015). Nutrient-Sensing Mechanisms across Evolution. Cell *161*, 67–83.

660 Christen, B., Abeliuk, E., Collier, J.M., Kalogeraki, V.S., Passarelli, B., Coller, J. a, Fero, M.J., McAdams, H.H., and Shapiro, L. (2011). The
661 essential genome of a bacterium. Mol. Syst. Biol. *7*, 528.

662 Costanzo, M., Baryshnikova, A., Bellay, J., Kim, Y., Spear, E.D., Sevier, C.S., Ding, H., Koh, J.L.Y., Toufighi, K., Mostafavi, S., et al. (2010). The
663 genetic landscape of a cell. Science *327*, 425–431.

664 Doerks, T., Copley, R.R., Schultz, J., Ponting, C.P., and Bork, P. (2002). Systematic identification of novel protein domain families associated
665 with nuclear functions. Genome Res *12*, 47–56.

666 Dubouloz, F., Deloche, O., Wanke, V., Cameroni, E., and De Virgilio, C. (2005). The TOR and EGO Protein Complexes Orchestrate
667 Microautophagy in Yeast. Mol. Cell *19*, 15–26.

668 Elbaz-Alon, Y., Rosenfeld-Gur, E., Shinder, V., Futerman, A.H., Geiger, T., and Schuldiner, M. (2014). A Dynamic Interface between Vacuoles
669 and Mitochondria in Yeast. Dev. Cell *30*, 95–102.

670 Ernst, R., Ejsing, C.S., and Antonny, B. (2016). Homeoviscous Adaptation and the Regulation of Membrane Lipids. J. Mol. Biol. *428*, 4776–
671 4791.

672 Giaever, G., Chu, A.M., Ni, L., Connelly, C., Riles, L., Véronneau, S., Dow, S., Lucau-Danila, A., Anderson, K., André, B., et al. (2002). Functional
673 profiling of the Saccharomyces cerevisiae genome. Nature *418*, 387–391.

674 Girgis, H.S., Liu, Y., Ryu, W.S., and Tavazoie, S. (2007). A comprehensive genetic characterization of bacterial motility. PLoS Genet. *3*, 1644–
675 1660.

676 Hall, M.N. (1996). The TOR signalling pathway and growth control in yeast. Biochem. Soc. Trans. *24*, 234–239.

677 Heitman, J., Movva, N.R., Hiestand, P.C., and Hall, M.N. (1991). FK 506-binding protein proline rotamase is a target for the
678 immunosuppressive agent FK 506 in Saccharomyces cerevisiae. Proc. Natl. Acad. Sci. U. S. A. *88*, 1948–1952.

679 Hönscher, C., Mari, M., Auffarth, K., Bohnert, M., Griffith, J., Geerts, W., van der Laan, M., Cabrera, M., Reggiori, F., and Ungermann, C.
680 (2014). Cellular Metabolism Regulates Contact Sites between Vacuoles and Mitochondria. Dev. Cell *30*, 86–94.

681   Hoppins, S., Collins, S.R., Cassidy-Stone, a., Hummel, E., DeVay, R.M., Lackner, L.L., Westermann, B., Schuldiner, M., Weissman, J.S., and
682   Nunnari, J. (2011). A mitochondrial-focused genetic interaction map reveals a scaffold-like complex required for inner membrane
683   organization in mitochondria. J. Cell Biol.

684   Ip, S.C.Y., Rass, U., Blanco, M.G., Flynn, H.R., Skehel, J.M., and West, S.C. (2008). Identification of Holliday junction resolvases from humans
685   and yeast. Nature *456*, 357–361.

686   Janke, C., Magiera, M.M., Rathfelder, N., Taxis, C., Reber, S., Maekawa, H., Moreno-Borchart, A., Doenges, G., Schwob, E., Schiebel, E., et al.
687   (2004). A versatile toolbox for PCR-based tagging of yeast genes: new fluorescent proteins, more markers and promoter substitution
688   cassettes. Yeast *21*, 947–962.

689   Jin, Q.W., Fuchs, J., and Loidl, J. (2000). Centromere clustering is a major determinant of yeast interphase nuclear organization. J. Cell Sci.
690   1903–1912.

691   Kim, A., and Cunningham, K.W. (2015). A LAPF/phafin1-like protein regulates TORC1 and lysosomal membrane permeabilization in
692   response to endoplasmic reticulum membrane stress. Mol. Biol. Cell *26*, 4631–4645.

693   Kornmann, B., Currie, E., Collins, S.R., Schuldiner, M., Nunnari, J., Weissman, J.S., and Walter, P. (2009). An ER-mitochondria tethering
694   complex revealed by a synthetic biology screen. Science *325*, 477–481.

695   Lang, A., John Peter, A.T., and Kornmann, B. (2015a). ER–mitochondria contact sites in yeast: beyond the myths of ERMES. Curr. Opin. Cell
696   Biol. *35*, 7–12.

697   Lang, A.B., John Peter, A.T., Walter, P., and Kornmann, B. (2015b). ER-mitochondrial junctions can be bypassed by dominant mutations in
698   the endosomal protein Vps13. J. Cell Biol. *210*, 883–890.

699   Lazarow, K., Du, M.-L., Weimer, R., and Kunze, R. (2012). A hyperactive transposase of the maize transposable element activator (Ac).
700   Genetics *191*, 747–756.

701   Lazarow, K., Doll, M.-L., and Kunze, R. (2013). Molecular biology of maize Ac/Ds elements: an overview. Methods Mol. Biol. *1057*, 59–82.

702   Lee, W., Tillo, D., Bray, N., Morse, R.H., Davis, R.W., Hughes, T.R., and Nislow, C. (2007). A high-resolution atlas of nucleosome occupancy in
703   yeast. Nat Genet *39*, 1235–1244.

704   Longtine, M.S., McKenzie, A., Demarini, D.J., Shah, N.G., Wach, A., Brachat, A., Philippsen, P., and Pringle, J.R. (1998). Additional modules
705   for versatile and economical PCR-based gene deletion and modification in Saccharomyces cerevisiae. Yeast *14*, 953–961.

706   Majumdar, S., Ghatak, J., Mukherji, S., Bhattacharjee, H., and Bhaduri, A. (2004). UDPgalactose 4-epimerase from Saccharomyces cerevisiae:
707   A bifunctional enzyme with aldose 1-epimerase activity. Eur. J. Biochem. *271*, 753–759.

708   Matos, J., Blanco, M.G., Maslen, S., Skehel, J.M., and West, S.C. (2011). Regulatory control of the resolution of DNA recombination
709   intermediates during meiosis and mitosis. Cell *147*, 158–172.

710   McMurray, M.A., Bertin, A., Garcia, G., Lam, L., Nogales, E., and Thorner, J. (2011). Septin Filament Formation Is Essential in Budding Yeast.
711   Dev. Cell *20*, 540–549.

712   Ölmezer, G., Levikova, M., Klein, D., Falquet, B., Fontana, G.A., Cejka, P., and Rass, U. (2016). Replication intermediates that escape Dna2
713   activity are processed by Holliday junction resolvase Yen1. Nat. Commun. *7*, 13157.

714   van Opijnen, T., Bodi, K.L., and Camilli, A. (2009). Tn-seq: high-throughput parallel sequencing for fitness and genetic interaction studies in
715   microorganisms. Nat. Methods *6*, 767–772.

716   Parsons, A.B., Brost, R.L., Ding, H., Li, Z., Zhang, C., Sheikh, B., Brown, G.W., Kane, P.M., Hughes, T.R., and Boone, C. (2004). Integration of
717   chemical-genetic and genetic interaction data links bioactive compounds to cellular target pathways. Nat. Biotechnol. *22*, 62–69.

718   Péli-Gulli, M.-P., Sardu, A., Panchaud, N., Raucci, S., and De Virgilio, C. (2015). Amino Acids Stimulate TORC1 through Lst4-Lst7, a GTPase-
719   Activating Protein Complex for the Rag Family GTPase Gtr2. Cell Rep. *13*, 1–7.

720   Powis, K., and De Virgilio, C. (2016). Conserved regulators of Rag GTPases orchestrate amino acid-dependent TORC1 signaling. Cell Discov. *2*,
721   15049.

722   Saba, J.D., Nara, F., Bielawska, A., Garrett, S., and Hannun, Y.A. (1997). The BST1 gene of Saccharomyces cerevisiae is the sphingosine-1-
723   phosphate lyase. J. Biol. Chem. *272*, 26087–26090.

724 Sanders, S.L., Garbett, K.A., and Weil, P.A. (2002). Molecular characterization of Saccharomyces cerevisiae TFIID. Mol. Cell. Biol. *22*, 6000–
725 6013.

726 Schuldiner, M., Collins, S.R., Thompson, N.J., Denic, V., Bhamidipati, A., Punna, T., Ihmels, J., Andrews, B.J., Boone, C., Greenblatt, J.F., et al.
727 (2005). Exploration of the function and organization of the yeast early secretory pathway through an epistatic miniarray profile. Cell *123*,
728 507–519.

729 Storici, F., and Resnick, M.A. (2003). Delitto perfetto targeted mutagenesis in yeast with oligonucleotides. Genet. Eng. (N. Y). *25*, 189–207.

730 Stracka, D., Jozefczuk, S., Rudroff, F., Sauer, U., and Hall, M.N. (2014). Nitrogen source activates TOR (target of rapamycin) complex 1 via
731 glutamine and independently of Gtr/Rag proteins. J. Biol. Chem. *289*, 25010–25020.

732 Tan, T., Ozbalci, C., Brügger, B., Rapaport, D., and Dimmer, K.S. (2013). Mcp1 and Mcp2, two novel proteins involved in mitochondrial lipid
733 homeostasis. J. Cell Sci. *126*, 3563–3574.

734 Teng, X., Dayhoff-Brannigan, M., Cheng, W.-C., Gilbert, C.E., Sing, C.N., Diny, N.L., Wheelan, S.J., Dunham, M.J., Boeke, J.D., Pineda, F.J., et
735 al. (2013). Genome-wide consequences of deleting any single gene. Mol. Cell *52*, 485–494.

736 Trotter, P.J., and Voelker, D.R. (1995). Identification of a non-mitochondrial phosphatidylserine decarboxylase activity (PSD2) in the yeast
737 Saccharomyces cerevisiae. J. Biol. Chem. *270*, 6062–6070.

738 Urban, J., Soulard, A., Huber, A., Lippman, S., Mukhopadhyay, D., Deloche, O., Wanke, V., Anrather, D., Ammerer, G., Riezman, H., et al.
739 (2007). Sch9 Is a Major Target of TORC1 in Saccharomyces cerevisiae. Mol. Cell *26*, 663–674.

740 Vollbrecht, E., Duvick, J., Schares, J.P., Ahern, K.R., Deewatthanawong, P., Xu, L., Conrad, L.J., Kikuchi, K., Kubinec, T.A., Hall, B.D., et al.
741 (2010). Genome-wide distribution of transposed Dissociation elements in maize. Plant Cell *22*, 1667–1685.

742 Wan, R., Yan, C., Bai, R., Huang, G., and Shi, Y. (2016). Structure of a yeast catalytic step I spliceosome at 3.4 Å resolution. Science *353*, 895–
743 904.

744 Weil, C.F., and Kunze, R. (2000). Transposition of maize Ac/Ds transposable elements in the yeast Saccharomyces cerevisiae. Nat. Genet. *26*,
745 187–190.

746 Weissman, J. (2010). Guide to Yeast Genetics: Functional Genomics, Proteomics, and Other Systems Analysis. In Methods in Enzymology, C.
747 Guthrie, and G. Fink, eds. p. 470.

748 Xie, M.W., Jin, F., Hwang, H., Hwang, S., Anand, V., Duncan, M.C., and Huang, J. (2005). Insights into TOR function and rapamycin response:
749 chemical genomic profiling by using a high-density cell array method. Proc. Natl. Acad. Sci. U. S. A. *102*, 7215–7220.

750 Zhang, X., Skrzypek, M.S., Lester, R.L., and Dickson, R.C. (2001). Elevation of endogenous sphingolipid long-chain base phosphates kills

751 Saccharomyces cerevisiae cells. Curr. Genet. *40*, 221–233.

752

753

Figure legends

Figure 1

Principle of the method.

A) Outline of the experimental procedure. Left, the transposon (green) can insert either into non-essential DNA (blue) and give rise to a clone, or into essential DNA (orange), in which case no clone is formed. Right, procedure to identify transposon insertion sites by deep-sequencing.

B) Profile of the transposon density across the whole genome, when the transposon original location is either a centromeric plasmid (top) or the endogenous *ADE2* locus on chromosome XV (bottom). The dashed lines indicate the chromosome centromeres.

C) Six examples of genomic regions and their corresponding transposon coverage in seven independent transposon libraries of indicated genotypes. Each vertical grey line represents one transposon insertion event. Genes annotated as essential are shown in orange, others in blue. Green arrowheads indicate the places where the absence of transposon coverage coincides with an essential gene.

D) Histogram of the number of transposons found in every annotated gene (CDS). The vertical dashed line is the median of the distribution.

E) Same as D, with genes categorized as non-essential (blue) and essential (orange) according to previous annotations.

Figure 1 – figure supplement 1

Size distribution of the colonies appearing on SD +Galactose -Ade. A) Histogram of colony area for a randomly chosen sample of 402 colonies. B) Example of picture of colonies (top) and segmentation thereof (bottom) used to calculate histogram in (A). Scale bar, 1 mm

Figure 1 - figure supplement 2

Genome-wide analysis of transposon insertion sites. A) Frequency plot of nucleotide composition around transposon insertion site. The strand is determined according to the orientation of the transposon insertion. Plot was calculated with a random sample of 50,000 transposon in the wild-type library 1. Note that GC-content of the yeast genome is 38%. B) Preferential transposon insertion into internucleosomal DNA. Three genomic regions are shown. For each, the top panel shows the nucleosomal density as determined in (Lee et al., 2007), and the bottom panels shows transposon insertion as in Figures 2-5. C) Correlation analysis of nucleosome and transposon density. Transposon densities were calculated on the wild-type library 1 by averaging transposon number within a 40 bp moving average. Top, correlation coefficient calculated between the nucleosome and the transposon data offset by the indicated number of bp. The correlation is most negative when offset=0. The periodicity is ~160 bp. Middle, autocorrelation of transposon data. The periodicity is identical as above. Bottom, autocorrelation of the nucleosome density data. The periodicity is identical as above. D) Analysis of transposon number relative to distance from centromere. For each chromosome, the number of transposons mapping within a certain distance from their respective centromere was computed and plotted (grey lines). The number of transposons increases linearly with the distance, except in the vicinity of the centromere, where transposon enrichment can be observed. The intercept of the linear regression, computed on the linear part of the plot and multiplied by 16 chromosomes, gives a rough estimate of the numbers of transposons enriched at pericentromeric regions (~20% of the total transposon number).

Figure 1 - figure supplement 3

Transposon density in essential and non-essential genes. As in Figure 1D-E, except that, for each gene, the transposon density (i.e. number of transposons divided by length of the gene) is shown.

Figure 2

800	Examples of genes showing partial loss of transposon coverage. The grey level is proportional to the
801	number of sequencing reads. Known functional domains are indicated.
802	A) Essential genes for which C-terminal truncations yield a viable phenotype.
803	B) Essential genes for which N-terminal truncations yield a viable phenotype.
804	C) Essential genes for which various truncations yield a viable phenotype.

Figure 2 - figure supplement 1

806	Detection of essential protein domains. Top, algorithm to detect essential protein domains.
807	This algorithm is implemented in MatLab Script 2. For each gene, a score is computed as
808	follows: the longest interval between transposon n and transposon n+5, multiplied by the
809	total number of transposons mapping to that gene, divided by the gene length to the
810	power of 1.5. A score of 0 is assigned to genes targeted by less than 20 transposons, in
811	which the longest interval is smaller than 300 bp, and/or in which the longest interval
812	represents more than 90% or less than 10% of the CDS length. Bottom, yeast genes sorted
813	according to their domain likelihood score. Vertical black bars above the graph indicate
814	previously annotated essential genes.

Figure 2 - figure supplement 2

| 816 | Transposon maps in the 100 highest scoring genes. Grey scale indicates the number of |
| 817 | sequencing reads as in Figure 2. |

Figure 2 - figure supplement 3

| 819 | Transposon maps in the genes scoring 101 to 200. |

Figure 2 - figure supplement 4

| 821 | Transposon maps in the genes scoring 201 to 300. |

Figure 2 - figure supplement 5

| 823 | Transposon maps in the genes scoring 301 to 400. |

Figure 3

824

825 *TAF3* and *PRP45* can be truncated without visible effects on cell growth.

826 A) A truncation of *TAF3* was generated in a heterozygous diploid strain (left) by introduction of an HA

827 tag and a G418-resistance cassette (HA kan'). The strain was tetrad dissected (middle). Tetrads 2 and

828 3 were further analyzed by PCR to confirm the mendelian segregation of the truncated allele (right).

829 B) A complete *TAF3* deletion was generated in a heterozygous diploid strain (left) by introduction of a

830 G418-resistance cassette (kan'). Meiosis yields only two viable, G418-sensitive spores per tetrad,

831 confirming that *TAF3* complete deletion is lethal.

832 C-D) As in (A-B) but applied to *PRP45*. Asterisks in the right panel designate PCR reactions that were

833 inefficient at amplifying the large truncated allele. The genotype of these spores can nevertheless be

834 inferred from the mendelian segregation of the G418 resistance.

835 E) Top, cryo-EM structure of the *S. cerevisiae* spliceosome (PDB accession 5GMK (Wan et al., 2016)).

836 Bottom, the same structure stripped of every protein except Prp45. The essential portion of Prp45 as

837 defined in (C) is in green and the non-essential part is in red and yellow. U2, U6, U5 and substrate

838 RNAs are depicted in pale blue, pink, dark blue and orange, respectively. The red circle indicates the

839 catalytic active site of the spliceosome.

840 F) Alignment of the Human, *S. cerevisiae*, and *S. pombe* Prp45 orthologs. The green, red and yellow boxes

841 are colored as in (E). The yellow box features the most conserved region of the protein.

Figure 4

842

843 Genetic interaction analyses. Libraries in panels B, C, E and G are displayed in the same order as in

844 Figure 1C.

845 A) Comparison of the number of transposons inserted in each of the 6603 yeast CDSs in the wild-type (x-

846   axis) and *mmm1Δ VPS13(D716H)* (y-axis) libraries.

847 B) Transposon coverage of genes encoding ERMES components is increased in libraries from strains

848   bearing the *VPS13(D716H)* allele.

849 C) Examples of genes showing synthetic sick/lethal interaction with *mmm1Δ VPS13(D716H)*.

850 D) Comparison of the number of transposons inserted in each of the 6603 yeast CDSs in the wild-type

851   (x-axis) and *dpl1Δ* (y-axis) libraries.

852 E) Transposon coverage of the *HIP1* locus in the *dpl1Δ his3Δ* library and in all the other libraries (*HIS3*).

853 F) Comparison of the number of transposons inserted in each of the 6603 yeast CDSs in the *dpl1Δ* (x-

854   axis) and *dpl1Δ psd2Δ* (y-axis) libraries.

855 G) Transposon coverage of the *PSD1* locus in the *dpl1Δ psd2Δ* and in all other libraries.

856 # Figure 4 – figure supplement 1

857   Volcano plots comparing libraries or combinations of libraries as indicated. The calculated fold-change

858   in transposon density between the two sets of libraries is plotted in $\log_2$ scale on the x-axis. The -

859     $\log_{10}$(p-value) (computed using the Student's t-test) is plotted on the y-axis. [1]The *VPS13(D716H)* and

860   the *mmm1Δ VPS13(D716H)* strains were generated in a *MET17* background while all other libraries

861   where generated in a *met17Δ* background. As a result *MET17* and the overlapping ORF *YLR302C*

862   appear as transposon free in the reference set. *MET6* is more targeted by transposons in *met17Δ*

863   libraries, likely because Met17 produces homocysteine, which needs to be converted to methionine by

864   Met6, or might otherwise accumulate to toxic levels. [2]The *VPS13(D716H)* and *mmm1Δ*

865   *VPS13(D716H) s*trains were generated in a Matα background, while the others were generated in a

866   Mata background. [3]*YGR190C* overlaps with *HIP1*. [4]*GPP1* shows synthetic lethality with a recessive

867   mendelian variant present in the *psd2Δ dpl1Δ* strain. However, this variant is neither linked to *DPL1*

868   nor to *PSD2* (data not shown). [5]ERMES component genes scores very high with respect to fold

869   change, because two of the five libraries in the reference set bear the *VPS13(D716H)* allele. The *p*-

870   value, by contrast, is not significant.

871   Figure 5

872   Synthetic rescue of lethal phenotypes

873   A) Transposon coverage of *CDC10* in the seven libraries. The coverage is increased in the *dpl1Δ psd2Δ*

874   library.

875   B) Tetrad dissection of a *PSD2/psd2Δ DPL1/dpl1Δ CDC10/cdc10Δ* triple heterozygote at 30℃ (left) and

876   25℃ (right). The *cdc10Δ* spores of ascertained genotype are circled with a color-coded solid line.

877   *cdc10Δ* spores for which the genotype can be inferred from the other spores of the tetrad are circled

878   with a color-coded dashed line.

879   C) Quantification of growing and non-growing *cdc10Δ* spores of the indicated genotype obtained

880   from 48 tetrads (three independent diploids).

881   D) Transposon coverage of *DNA2* in the seven libraries. The coverage is increased in the *YEN1^{on}* library.

882   E) Tetrad dissection of a *DNA2/dna2Δ YEN1/YEN1* single heterozygote and of a *DNA2/dna2Δ*

883   *YEN1/YEN1^{on}* double heterozygote at 30℃ (left) and 25℃ (right). All viable *dna2Δ* spores additionally

884   carry the *YEN1^{on}* allele (red circle).

885   F) FACS profile of propidium-iodide-stained DNA content in DNA2 and *dna2Δ YEN1^{on}* strains

886   exponentially growing at 30℃ (left) and 25℃ (right). For *DNA2* panels, each profile is an overlay of

887   two independent strains. For *dna2Δ YEN1^{on}* panels, each profile is an overlay of four independent

888   strains.

Figure 6

890   Detection of rapamycin resistant strains.

891   A)   Comparison of the number of sequencing reads mapping to each of the 6603 yeast CDSs in

892   rapamycin-untreated (x-axis) and -treated (y-axis) libraries. Note the difference in scale between

893   both axis due to the high representation of rapamycin-resistant clones.

894   B)   Distribution of transposons and number of associated sequencing reads on the *PIB2* gene.

895   Transposons with high number of sequencing reads in the rapamycin-treated library are clustered at

896   the 5'-end of the CDS.

897   C)   Wild-type (WT) and *pib2Δ* strains were transformed with either an empty plasmid (⊠) or plasmids

898   encoding full-length (FL) or indicated fragments of Pib2 (see E, numbers refer to the amino acid

899   position in the full-length Pib2 protein). 5-fold serial dilutions of these strains were spotted on YPD

900   or YPD containing 10 ng/ml rapamycin. Centromeric plasmids were used in all strains, except in

901   those denoted with 2μ, which carried multi-copy plasmids.

902   D)   Strains of the indicated genotypes, transformed with either an empty plasmid (⊠) or plasmids

903   encoding full length (*pPIB2*) or truncated (*pPIB2$^{165-635}$*) versions of Pib2, were grown exponentially in

904   minimal medium with proline as nitrogen source. 3 mM glutamine was added to the culture and the

905   cells were harvested 2 minutes later. Protein extracts were resolved on an SDS-page and probed

906   with antibodies either specific for Sch9-pThr^{737} (P-Sch9), or for total Sch9 to assess TORC1 activity.

907   E)   Schematic overview of Pib2 architecture and of the fragments used for genetic studies.

908   F)   Summary of yeast-two-hybrid interactions between Pib2 fragments and the TORC1 subunit Kog1

909   (Figure 6 – figure supplement 1). Fragments indicated by a black box interacted with Kog1,

910   fragments indicated by a white box did not.

911   G) *pib2Δ* cells expressing the indicated Pib2 fragments from plasmids (see E) were assayed for their

912   sensitivity to rapamycin (2.5 or 5 ng/ml) as in C.

913   H) WT or *pib2Δ* cells expressing the indicated Pib2 fragments from plasmids were asseyed as in G,

914   except that cells were spotted on synthetic medium to apply a selective pressure for plasmid

915   maintenance.

Figure 6 – figure supplement 1

917   A) Transposon coverage of the *PIB2* gene. Top row is the rapamycin treated library and rows below

918   are presented as in Figure 2-5. The gray scale has been adjusted to account for the large number of

919   sequencing reads mapping in the 5' region of the gene.

920   B) Yeast-two-hybrid assay assessing the interaction of the indicated Pib2 fragments encoded on the

921   pCAB plasmid, with full-length Kog1 encoded on the pPR3N plasmid.

922   C) *gtr1Δ gtr2Δ* cells expressing indicated, plasmid-encoded Pib2 fragments (see Figure 6E) were

923   assayed for their sensitivity to rapamycin. Note that expressing Pib2$^{Δ533-620}$ in *gtr1Δ gtr2Δ* cells appears

924   to inhibit growth even in the absence of rapamycin.

925   D) *gtr1Δ gtr2Δ* cells, transformed with centromeric plasmids expressing Pib2 fragments (see Figure

926   6E) and alleles of Gtr1 and Gtr2 as indicated, were assayed for their sensitivity to rapamycin.

Supplementary File 1

928   Processed dataset containing (1) the position and number of reads for all transposons in each library

929   (in the WIG format),

930   • Processed dataset - Dpl1del.wig
931   • Processed dataset - Mmm1Del_Vps13D716H.wig
932   • Processed dataset - Psd2Del_Dpl1del.wig
933   • Processed dataset - V13D716H.wig

934 • Processed dataset - WildType1.wig
935 • Processed dataset - WildType2.wig
936 • Processed dataset - WT_plus_rapamycin.wig
937 • Processed dataset - Yen1on.wig

938 (2) summaries of the number of transposon and number of reads per gene, for all genes in each

939 library (in the TXT format).

940 • Processed dataset - Dpl1del_pergene.txt
941 • Processed dataset - Mmm1Del_Vps13D716H_pergene.txt
942 • Processed dataset - Psd2Del_Dpl1del_pergene.txt
943 • Processed dataset - V13D716H_pergene.txt
944 • Processed dataset - WildType1_pergene.txt
945 • Processed dataset - WildType2_pergene.txt
946 • Processed dataset - WT_plus_rapamycin_pergene.txt
947 • Processed dataset - Yen1on_pergene.txt

948

949 ## Supplementary File 2

950 Table of genes appearing as essential in our analysis (i.e., their density of transposon is below 1/400

951 bp), but were not previously annotated as essential. The likely explanation for the low transposon

952 density is written in column B for each gene.

953 ## Supplementary File 3

954 Data computed to draw the volcano plots (Figure 4 – figure supplement 1)

955

Tables

Table 1: Characteristics of the libraries

library	Number of colonies	reads mapped	transposons mapped	median read per transposon	number of MiSeq runs	overlap between MiSeq runs
Wild-type 1	~1.6×10^6	31794831	284162	22	$2^{(1)}$	54%, 88%[1]
Wild-type 2	~2.4×10^6	15303285	258568	12	1	NA
VPS13(D716H)	~4.7×10^6	24958456	414114	13	$2^{(2)}$	41%, 42%[2]
Mmm1Δ VPS13(D716H)	~1.9×10^6	17799948	303323	12	1	NA
dpl1Δ	~2.3×10^6	15077156	401126	8	1	NA
dpl1Δ psd2Δ	~2.9×10^6	11649561	363179	9	1	NA
YEN1^{on}	~2.8×10^6	9517877	495125	6	1	NA
Wild-type 2 + rapamycin	~2.4×10^6	9664956	169322	9	1	NA

[1] The harvested library was grown in two flasks, one at 30°C and the other at 37°C. DNA was extracted separately from the two cultures and sequenced in two separate MiSeq runs

[2] The library was harvested as ten subpools, which were grown in ten separate flasks. DNA was extracted separately. In one case, DNA from all ten subpools was pooled and processed to sequencing in one MiSeq run. In the other case, DNAs were kept separate and processed until the PCR step (1x 100 µl PCR by subpool). PCR products were pooled and sequenced as another MiSeq run.

966   Table 2: Yeast strains used in this study.

Name	Parent	Genotype	Reference
CWY1	BY4723	*MATa his3Δ0 ura3Δ0 ade2:Ds-1*	Weil et al., 2000
ByK157	BY4743	*MATa his3Δ1 leu2Δ0 lys2Δ0 ura3Δ0 VPS13(D716H)*	Lang et al. 2015
ByK352	BY4741	*MATa his3Δ1 leu2Δ0 met17Δ0 ura3Δ0 ade2Δ::HIS3**	This study
ByK484	By4742	*MATa his3Δ1 leu2Δ0 lys2Δ0 ura3Δ0 ade2Δ::HIS3**	This study
ByK485	ByK352 and ByK484	*MATa/α his3Δ1/his3Δ1 leu2Δ0/leu2Δ0 LYS2/lys2Δ0 met17Δ0/MET17 ura3Δ0/ura3Δ0 ade2Δ::HIS3*/ade2Δ::HIS3**	This study
ByK446	ByK157	*MATa his3Δ1 leu2Δ0 ura3Δ0 ade2Δ::HIS3* VPS13(D716H)*	This study
ByK528	ByK446	*MATa his3Δ1 leu2Δ0 ura3Δ0 ade2Δ::HIS3* VPS13(D716H) mmm1Δ::KanMX6*	This study
ByK530	ByK352	*MATa his3Δ1 leu2Δ0 met17Δ0 ura3Δ0 ade2Δ::NAT* dpl1Δ::KanMX6*	This study
ByK533	ByK352	*MATa his3Δ1 leu2Δ0 met17Δ0 ura3Δ0 ade2Δ::HIS3* psd2Δ::KanMX6 dpl1Δ::NAT*	This study
ByK576	ByK485	*MATa/α his3Δ1/his3Δ1 leu2Δ0/leu2Δ0 LYS2/lys2Δ0 met17Δ0/MET17 ura3Δ0/ura3Δ0 ade2Δ::HIS3*/ade2Δ::HIS3* prp45Δ::KanMX6/PRP45*	This study
ByK579	ByK485	*MATa/α his3Δ1/his3Δ1 leu2Δ0/leu2Δ0 LYS2/lys2Δ0 met17Δ0/MET17 ura3Δ0/ura3Δ0 ade2Δ::HIS3*/ade2Δ::HIS3* PRP45$^{1\text{-}462}$-HA(KanMX6)/ PRP45*	This study
ByK583	ByK485	*MATa/α his3Δ1/his3Δ1 leu2Δ0/leu2Δ0 LYS2/lys2Δ0 met17Δ0/MET17 ura3Δ0/ura3Δ0 ade2Δ::HIS3*/ade2Δ::HIS3* taf3Δ::KanMX6/TAF3*	This study
ByK588	ByK485	*MATa/α his3Δ1/his3Δ1 leu2Δ0/leu2Δ0 LYS2/lys2Δ0 met17Δ0/MET17 ura3Δ0/ura3Δ0 ade2Δ::HIS3*/ade2Δ::HIS3* TAF3$^{1\text{-}270}$-HA(KanMX6)/ TAF3*	This study
ByK725	ByK533 and ByK484	*MATa/α his3Δ1/his3Δ1 leu2Δ0/leu2Δ0 LYS2/lys2Δ0 met17Δ0/MET17 ura3Δ0/ura3Δ0 ade2Δ::HIS3*/ade2Δ::HIS3* psd2Δ::KanMX6/PSD2 dpl1Δ::NAT /DPL1*	This study
ByK726	ByK533 and ByK484	*MATa/α his3Δ1/his3Δ1 leu2Δ0/leu2Δ0 LYS2/lys2Δ0 met17Δ0/MET17 ura3Δ0/ura3Δ0 ade2Δ::HIS3*/ade2Δ::HIS3* psd2Δ::KanMX6/PSD2 dpl1Δ::NAT /DPL1*	This study
ByK739	ByK725	*MATa/α his3Δ1/his3Δ1 leu2Δ0/leu2Δ0 LYS2/lys2Δ0 met17Δ0/MET17 ura3Δ0/ura3Δ0 ade2Δ::HIS3*/ade2Δ::HIS3* psd2Δ::KanMX6/PSD2 dpl1Δ::NAT /DPL1 cdc10Δ::URA3/CDC10*	This study
ByK740	ByK726	*MATa/α his3Δ1/his3Δ1 leu2Δ0/leu2Δ0 LYS2/lys2Δ0 met17Δ0/MET17 ura3Δ0/ura3Δ0 ade2Δ::HIS3*/ade2Δ::HIS3* psd2Δ::KanMX6/PSD2 dpl1Δ::NAT /DPL1 cdc10Δ::URA3/CDC10*	This study
ByK741	ByK726	*MATa/α his3Δ1/his3Δ1 leu2Δ0/leu2Δ0 LYS2/lys2Δ0 met17Δ0/MET17 ura3Δ0/ura3Δ0 ade2Δ::HIS3*/ade2Δ::HIS3* psd2Δ::KanMX6/PSD2 dpl1Δ::NAT /DPL1 cdc10Δ::URA3/CDC10*	This study
YJM3916	ByK352	*MATa his3Δ1 leu2Δ0 met17Δ0 ura3Δ0 ade2Δ::HIS3* YEN1^{on}*	This study
YL516	BY4741/BY4742	*MATa his3Δ1 leu2Δ0 ura3Δ0*	Binda et al, 2009
MB32	YL516	*MATa his3Δ1 leu2Δ0 ura3Δ0 gtr1Δ::kanMX*	Binda et al, 2009
RKH106	YL516	*MATa his3Δ1 leu2Δ0 ura3Δ0 pib2Δ::kanMX*	This study
RKH241	MB32	*MATa his3Δ1 leu2Δ0 ura3Δ0 gtr1Δ::kanMX gtr2Δ::hphMX4*	This study
NMY51		*his3Δ200 trp1-901 leu2-3,112 ade2 LYS::(lexAop)4-HIS3 ura3::(lexAop)8- lacZ ade2::(lexAop)8-ADE2 GAL4*	Dualsystems Biotech AG

967   *ADE2 deleted -56 before ATG + 62 after STOP with PCR primers #6 and #7 on pFA6a-His3MX6.

968   Table 3: Oligonucleotides used in this study.

969

#	Original name	Sequence	Purpose
1	P5_MiniDs	AATGATACGGCGACCACCGAGATCTACtccgtcccgcaagttaaata	amplify library
2	MiniDs_P7	CAAGCAGAAGACGGCATACGAGATacgaaaacgaacgggataaa	amplify library
3	688_minidsSEQ1210	tttaccgaccgttaccgaccgttttcatcccta	sequence library
4	ADE2Fwd	GGTTCGAGCTCCCTTTTGATGCGGAATTGAC	clone *ADE2* MiniDS
5	ADE2Rev	GACCTGAGCTCTTACTGGATATGTATGTATG	clone *ADE2* MiniDS
6	Ade2PriFwd	GTATAAATTGGTGCGTAAAATCGTTGGATCTCTCTTCTAAcggatccccgggttaattaa	delete *ADE2*
7	Ade2PriRev	TATGTATGAAGTCCACATTTGATGTAATCATAACAAAGCCgaattcgagctcgtttaaac	delete *ADE2*
8	Dpl1_Janke_S1	AGCAAGTAGGCTAGCTTCTGTAAAGGGATTTTTCCATCTAATACAcgtacgctgcaggtcgac	delete *DPL1*
9	Dpl1_Janke_S2	GCACTCTCGTTCTTTAAATTATGTATGAGATTTGATTCTATATAGatcgatgaattcgagctcg	delete *DPL1*
10	Psd2_pringle_F	GATGCTGTATCAATTGGTAAAGAATCCTCGATTTTCAGGAGCATCCAACGcgtacgctgcaggtcgac	delete *PSD2*
11	Psd2_pringle_R	CTTGTTTGTACACGCTATAGTCTATAATAAAGTCTGAGGGAGATTGTTCATGatcgatgaattcgagctcg	delete *PSD2*
12	TAF3_R1	TGGATGAGATAATGACGAAAGAAAATGCAGAAATGTCGTTgaattcgagctcgtttaaac	*TAF3* partial deletion
13	TAF3_aa90_F2	AGGTATTGTTAAGCCTACGAACGTTCTGGATGTCTATGATcggatccccgggttaattaa	TAF3 partial deletion
14	Taf3_Fwd	GGCAAGATGTGATCAGGACG	check *TAF3* partial deletion
15	Taf3_Rev	TCTTGAAGAAGCGAAAGTACACT	check *TAF3* partial deletion
16	TAF3_R1	TGGATGAGATAATGACGAAAGAAAATGCAGAAATGTCGTTgaattcgagctcgtttaaac	*TAF3* complete deletion
17	TAF3_aa1_F1	GAAAACAGCGATATCTTTGGGTCAATAGAGTTCCTCTGCTtgaggcgcgccacttctaaa	*TAF3* complete deletion
18	PRP45_R1	ACTCAAGCACAAGAATGCTTTGTTTTCCTAGTGCTCATCCTGGGCgaattcgagctcgtttaaac	*PRP45* partial deletion
19	PRP45_aa154_F2	AACGACGAAGTCGTGCCTGTTCTCCATATGGATGGCAGCAATGATcggatccccgggttaattaa	*PRP45* partial deletion
20	PRP45_Fwd	AGGTTGTAGCACCCACAGAA	check *PRP45* partial deletion
21	PRP45_Rev	CAATCATCACACCTCAGCGA	check *PRP45* partial deletion
22	PRP45_R1	ACTCAAGCACAAGAATGCTTTGTTTTCCTAGTGCTCATCCTGGGCgaattcgagctcgtttaaac	*PRP45* complete deletion
23	PRP45_aa1_F1	GCTCTGAGCCGAGAGGACGTATCAGCAACCTCAACCAAATtgaggcgcgccacttctaaa	*PRP45* complete deletion
24	CDC10-Ura3_fwd	AAGGCCAAGCCCCACGGTTACTACAAGCACTCTATAAATATATTAtgacggtgaaaacctctgac	*CDC10* complete deletion
25	URA3-CDC10_rev	TTCTTAATAACATAAGATATATAATCACCACCATTCTTATGAGATtcctgatgcggtattttctcc	*CDC10* complete deletion
26	OJM370	ATGGGTGTCTCACAAATATGGG	Amplify *YEN1*
27	OJM371	TTCAATAGTGCTACTGCTATCAC	Amplify *YEN1*
28	OJM372	TTCAATAGTGCTACTGCTATCACTGTCACAGGCTCAAACCGGTCGACTG TTCGTACGCTGCAGGTCGAC	*Delitto perfetto* on *YEN1*
29	OJM373	ATGGGTGTCTCACAAATATGGGAATTTTTGAAGCCATATCTGCAAGATTCCCGCGCGTTGGCCGATT CAT	*Delitto perfetto* on *YEN1*
30	o3958	gacggtatcgataagcttgatatcgGCGCTGGCATCTTTAATCTC	*PIB2* cloning
31	o3959	actagtggatcccccgggctgcaggTGCTTGGATCCTTCTTGGTC	*PIB2* cloning
32	o3224	TAATA CGACT CACTA TAGGG	various *PIB2* truncations
33	o3225	ATTAA CCCTC ACTAA AGGGA A	various *PIB2* truncations
34	o4034	atctagttcagggttcgacattctggtctccactac	*PIB2*^165-635 truncation
35	o4010	gtagtggagaccagaatgtcgaaccctgaactagat	*PIB2*^165-635 truncation
36	o4012	tagtggagaccagaatgttaccgcagcctgct	*PIB2*^304-635 truncation
37	o4035	tcaaattagaactagcattcattctggtctccactacaactgtg	*PIB2*^221-635 truncation
38	o4011	cacagttgtagtggagaccagaatgaatgctagttctaatttga	*PIB2*^221-635 truncation
39	o4062	atagttggtattaagttgattctcattctggtctccactacaactg	*PIB2*^426-635 truncation
40	o3996	cagttgtagtggagaccagaatgagaatcaacttaataccaactat	*PIB2*^426-635 truncation
41	o4063	cgtgtttgcgttatggttgtcgctgttcggaataga	*PIB2*^Δ426-532 truncation
42	o3997	tctattccgaacagcgacaaccataacgcaaacacg	*PIB2*^Δ426-532 truncation
43	o4064	cacagagccgataacactcgtggttgaaaggttctc	*PIB2*^Δ533-620 truncation
44	o3998	gagaacctttcaaccacgagtgttatcggctctgtg	*PIB2*^Δ533-620 truncation
45	o4065	gtctcgcaaaaaatgttcatcagcccaaaacatcattaccttct	*PIB2*^1-620 truncation
46	o3999	agaaggtaatgatgttttgggctgatgaacatttttttgcgagac	*PIB2*^1-620 truncation
47	o1440	GCTAGAGCGGCCATTACGGCCCCGGAGATTTATGGACCTC	*KOG1* cloning into pPR3N
48	o1442	CGATCTCGGGCCGAGGCGGCCTCAAAAATAATCAATTCTCTCGTC	*KOG1* cloning into pPR3N
49	o3787	GCTAGAGCGGCCATTACGGCC GAATTGTACAAATCTAGAACTAGT	cloning *PIB2* fragments into pCabWT*
50	o3788	CGATCTCGGGCCGAGGCGGCCAA GAAACTACTCCAATTCCAGTTTGC	cloning *PIB2* fragments into pCabWT*
51	o3872	CGATCTCGGGCCGAGGCGGCCAAGCCCAAAACATCATTACCTTCTTCT	cloning *PIB2* fragments into pCabWT*
52	o3871	CGATCTCGGGCCGAGGCGGCCAAATCTTCGCCCTCCTCAACGT	cloning *PIB2* fragments into pCabWT*
53	o3870	CGATCTCGGGCCGAGGCGGCCAAGTTGATTCTGTCGCTGTTCG	cloning *PIB2* fragments into pCabWT*
54	o3933	GCTAGAGCGGCCATTACGGCCAGGAAGAAATTACGCAATTACTAC	cloning *PIB2* fragments into pCabWT*

44

55	o3934	GCTAGAGCGGCCATTACGGCC AGTGTTATCGGCTCTGTGCC	cloning *PIB2* fragments into pCabWT*
56	o3868	CGATCTCGGGCCGAGGCGGCCAAATTAGTGCTCGAAGCAGGCT	cloning *PIB2* fragments into pCabWT*
57	o3867	CGATCTCGGGCCGAGGCGGCCAAGTCATCCGTGAATGGCAACG	cloning *PIB2* fragments into pCabWT*
58	o3866	CGATCTCGGGCCGAGGCGGCCAAGCCTGCCCCTGTTGAGCTCT	cloning *PIB2* fragments into pCabWT*
59	o3865	CGATCTCGGGCCGAGGCGGCCAAGTCAGCACCGCTTTCCTCAT	cloning *PIB2* fragments into pCabWT*

970   Oligonucleotides #1 and #2, ordered as PAGE-purified and lyophilized, are resuspended at 100 µM in

971   water. Oligonucleotide #3, ordered as HPLC-purified and lyophilized, is resuspended at 100 µM in

972   water and distributed into single-use aliquots.

973

Table 4: Plasmids used in this study.

| Name	Parent	Description	Reference
pBK257	pWL80R_4x	CEN/URA3, carries MiniDs in ADE2 and hyperactive Ac transposase under GAL1 promoter	This study
pWL80R_4x		CEN/URA3, carries hyperactive Ac transposase under GAL1 promoter	Lazarow et al. 2012
pCORE-UH		*Delitto pefetto* URA3 cassette	Storici et al. 2003
pJM7		pENTRY-*YEN1^{ON}*	This study
pRS413		*CEN/HIS3*, empty vector	Sikorski et al., 1989
pRS415		*CEN/LEU2*, empty vector	Sikorski et al., 1989
pRS416		*CEN/URA3*, empty vector	Sikorski et al., 1989
p1822	pRS413	*CEN/HIS3, GTR1*	This study
p1451	pRS415	*CEN/LEU2, GTR2*	This study
p1821	pRS413	*CEN/HIS3, GTR1^{Q65L}*	This study
p1452	pRS415	*CEN/LEU2, GTR2^{S23L}*	This study
p3084	pRS416	*CEN/URA3, PIB2*	This study
p3099	p3084	*CEN/URA3, PIB2^{165-635}*	This study
p3097	p3084	*CEN/URA3, PIB2^{304-635}*	This study
p3101	p3084	*CEN/URA3, PIB2^{221-635}*	This study
p3253	pRS426	*2μ/URA3, PIB2*	This study
p3255	pRS426	*2μ/URA3, PIB2^{165-635}*	This study
p3163	p3084	*CEN/URA3, PIB2^{426-635}*	This study
p3153	p3084	*CEN/URA3, PIB2^{Δ426-532}*	This study
p3154	p3084	*CEN/URA3, PIB2^{Δ533-620}*	This study
p3156	p3084	*CEN/URA3, PIB2^{1-620}*	This study
pPR3N		*2μ/TRP1, NubG-HA*	Dualsystems Biotech AG
pCabWT		*CEN/LEU2, Aβ-Cub-LexA-VP16*	Dualsystems Biotech AG
p3081	pPR3N	*2μ/TRP1, NubG-HA-KOG1*	This study
p2966	pCabWT	*CEN/LEU2, Aβ-PIB2-Cub-LexA-VP16*	This study
p3002	pCabWT	*CEN/LEU2, Aβ-PIB2^{1-620}-Cub-LexA-VP16*	This study
p3007	pCabWT	*CEN/LEU2, Aβ-PIB2^{1-550}-Cub-LexA-VP16*	This study
p3001	pCabWT	*CEN/LEU2, Aβ-PIB2^{1-428}-Cub-LexA-VP16*	This study
p3051	pCabWT	*CEN/LEU2, Aβ-PIB2^{440-550}-Cub-LexA-VP16*	This study
p3054	pCabWT	*CEN/LEU2, Aβ-PIB2^{556-620}-Cub-LexA-VP16*	This study
p3052	pCabWT	*CEN/LEU2, Aβ-PIB2^{621-635}-Cub-LexA-VP16*	This study
p3000	pCabWT	*CEN/LEU2, Aβ-PIB2^{1-312}-Cub-LexA-VP16*	This study
p2987	pCabWT	*CEN/LEU2, Aβ-PIB2^{304-635}-Cub-LexA-VP16*	This study
p2999	pCabWT	*CEN/LEU2, Aβ-PIB2^{1-162}-Cub-LexA-VP16*	This study
p2986	pCabWT	*CEN/LEU2, Aβ-PIB2^{165-635}-Cub-LexA-VP16*	This study
p2998	pCabWT	*CEN/LEU2, Aβ-PIB2^{1-101}-Cub-LexA-VP16*	This study
p2991	pCabWT	*CEN/LEU2, Aβ-PIB2^{102-635}-Cub-LexA-VP16*	This study
p2997	pCabWT	*CEN/LEU2, Aβ-PIB2^{1-49}-Cub-LexA-VP16*	This study
p2990	pCabWT	*CEN/LEU2, Aβ-PIB2^{50-635}-Cub-LexA-VP16*	This study

974
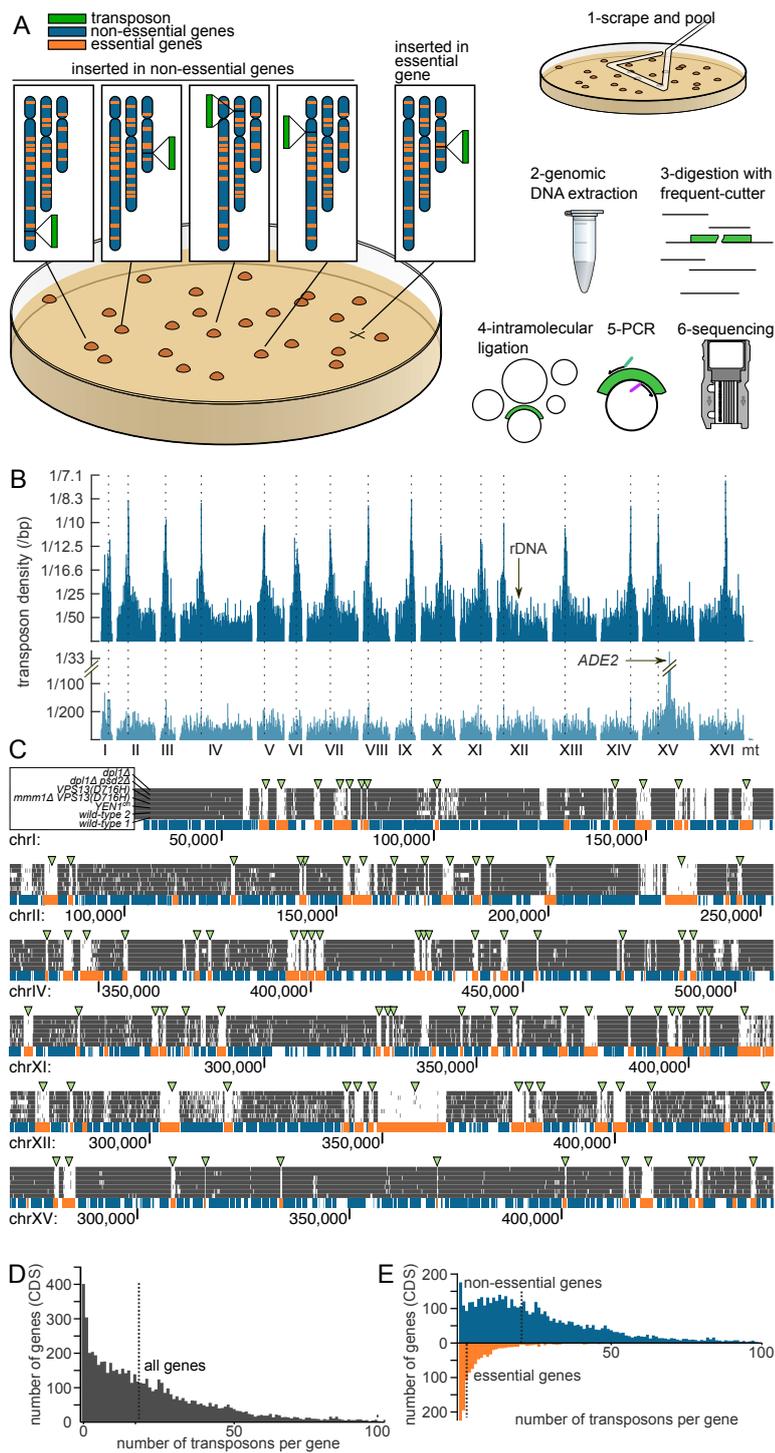
Figure 1

Figure 1 Supplement 1
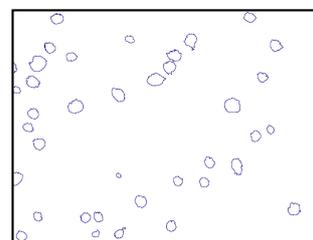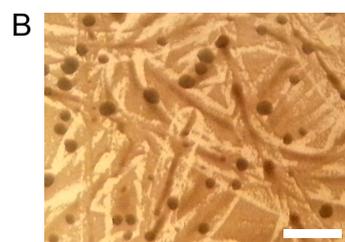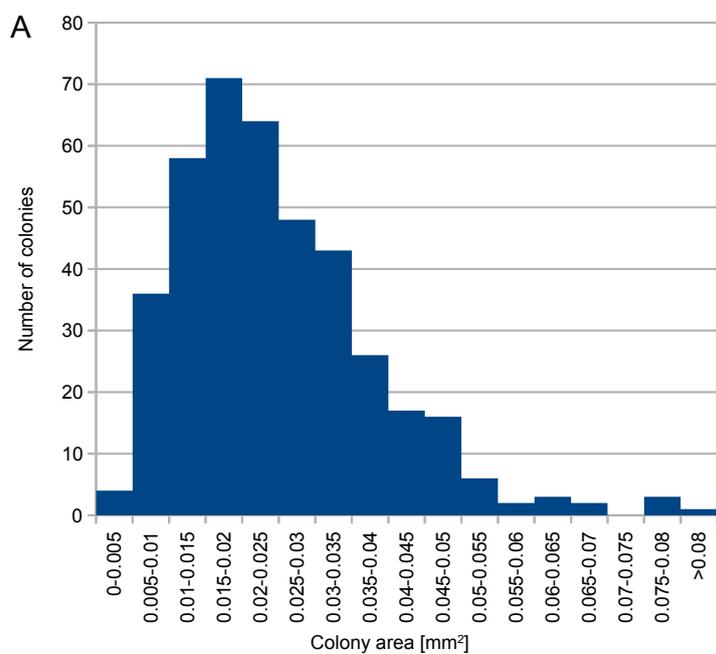
Figure 1 Supplement 2
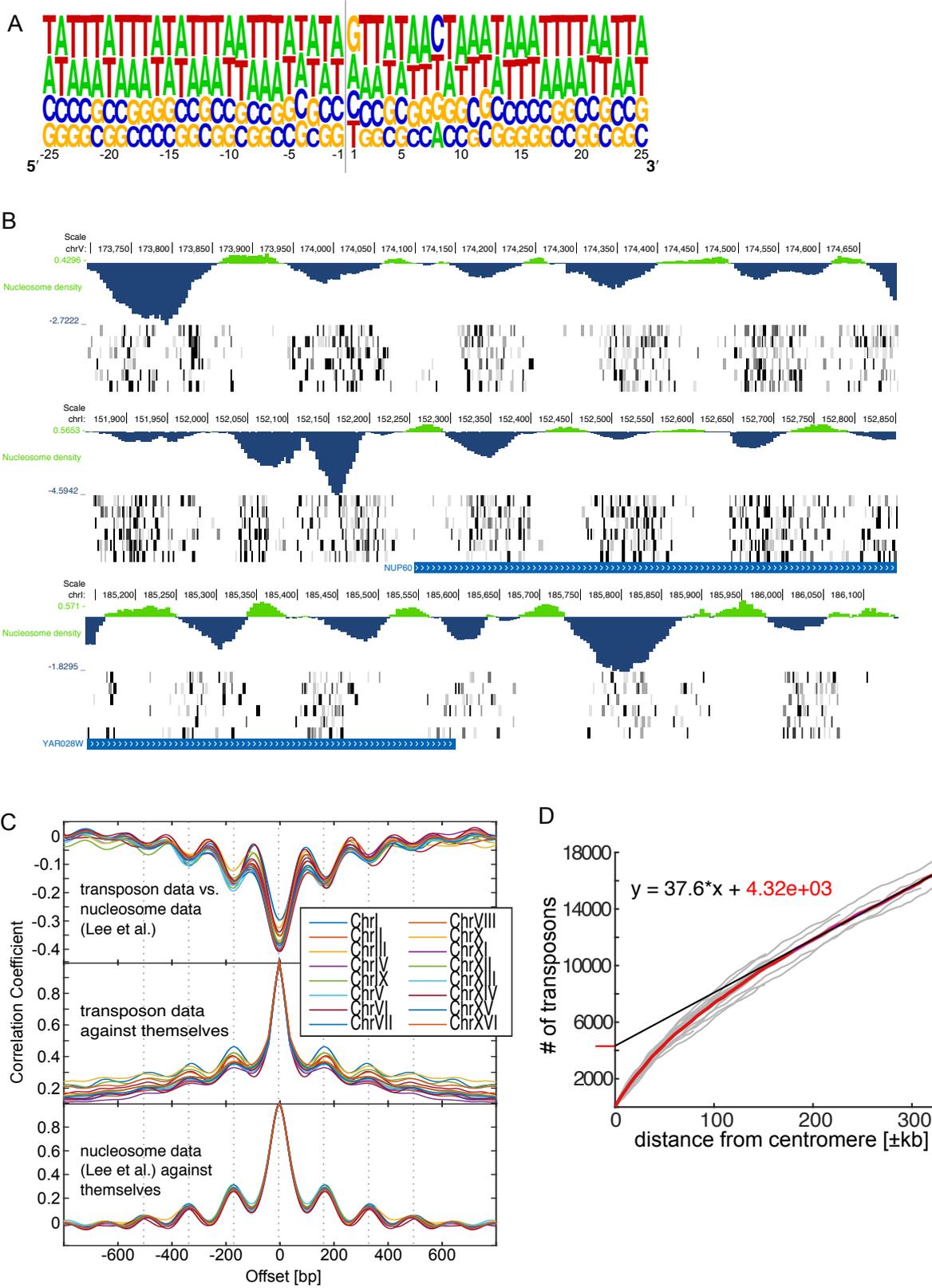
Figure 1 Supplement 3
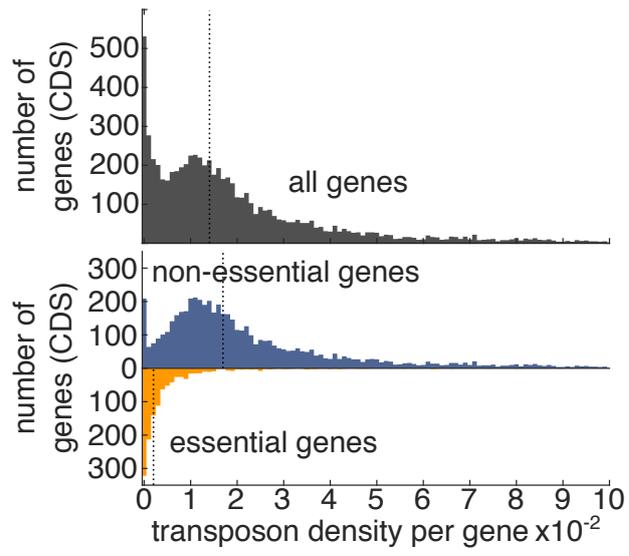
Figure 2

A C-terminal truncations

GAL10 — epimerase | mutarotase

ULP2 — catalytic

SEC12 — TM

SGV1 — kinase

MMS21 — RING

SEC8

RET2 — Clathrin adaptor | Mu_homology

HRR25 — kinase

NIC96

NPA3 — GTPase

MED6 — MED6 mediator subcomplex

APC11 — RING domain

B N-terminal truncations

TFC7 — phosphatase | TFIIIC

RIB2 — pseudoU synthase | deaminase

MOB1 — Mob1/phocein family

ULP1 — catalytic

PRP22 — S1-like | DEAH-box helicase

SRB4

PEP12 — syntaxin-like | SNARE

C mixed truncations

SEC9 — SNARE

PAN1 — EF | EF | Coil | Coil | DUF1720

SNU71 — PWI

SWI1 — ARID

FAB1 — FYVE | TCP-1 family | Coil | PI4K

PTA1

Figure 2 Supplement 1

$$\text{Domain likelihood score} = \frac{\text{longest interval} * \text{tn\_number}}{\text{gene length}^{1.5}}$$

Domain likelihood score =0 IF tn_number <20
OR longest interval>90% of CDS
OR longest interval<10% of CDS
OR longest interval<300 bp
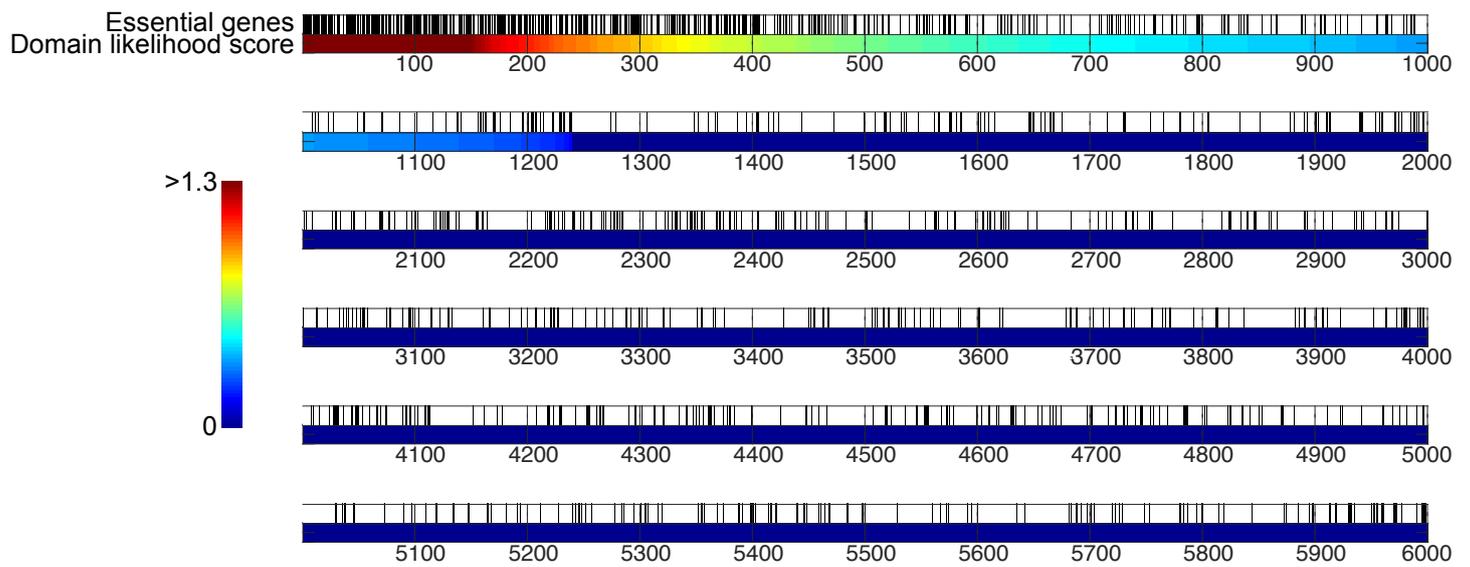
Figure 2 - supplement 2
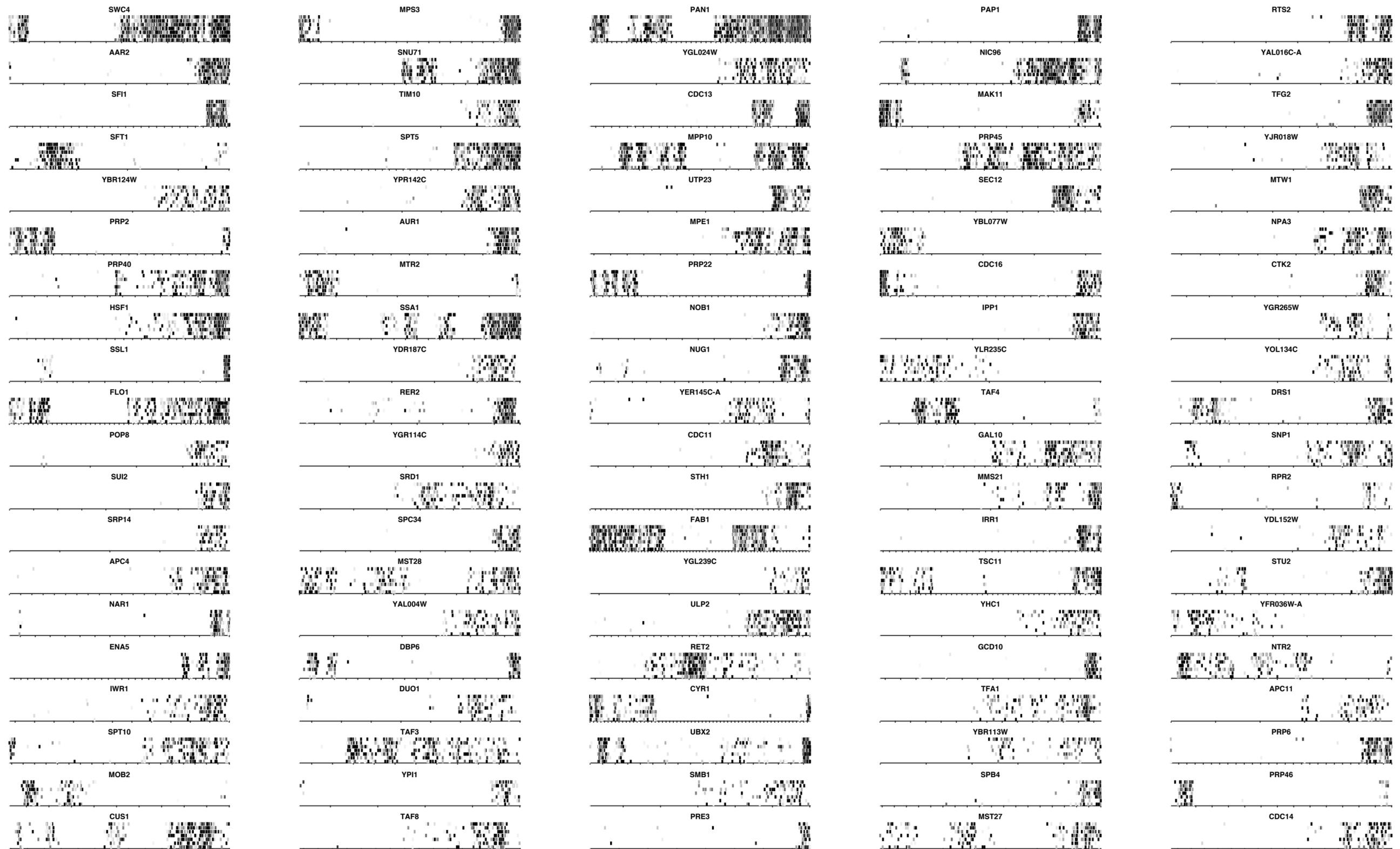
Figure 2 - supplement 3

Figure 2 - supplement 4
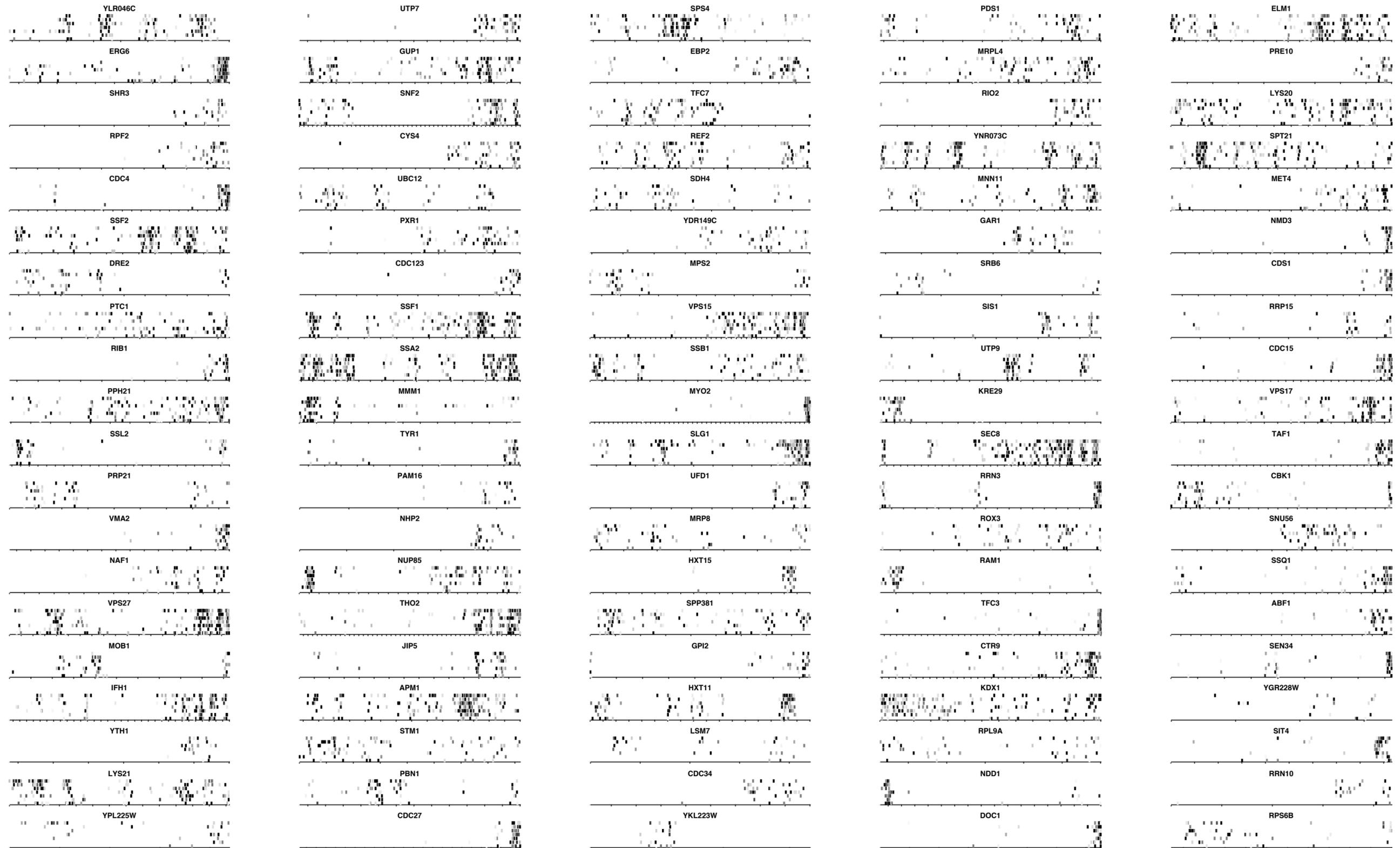
Figure 2 - supplement 5

Figure 3
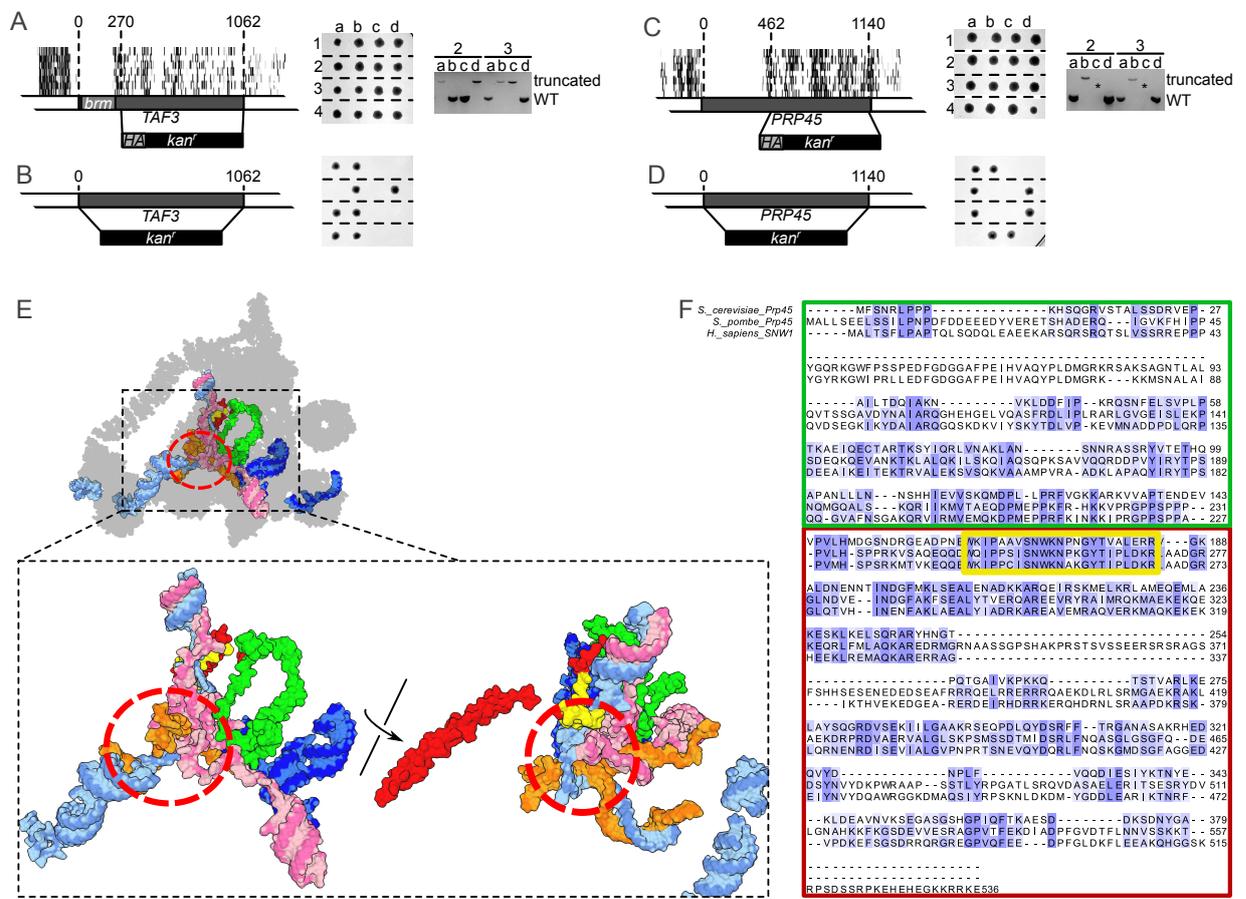
Figure 4
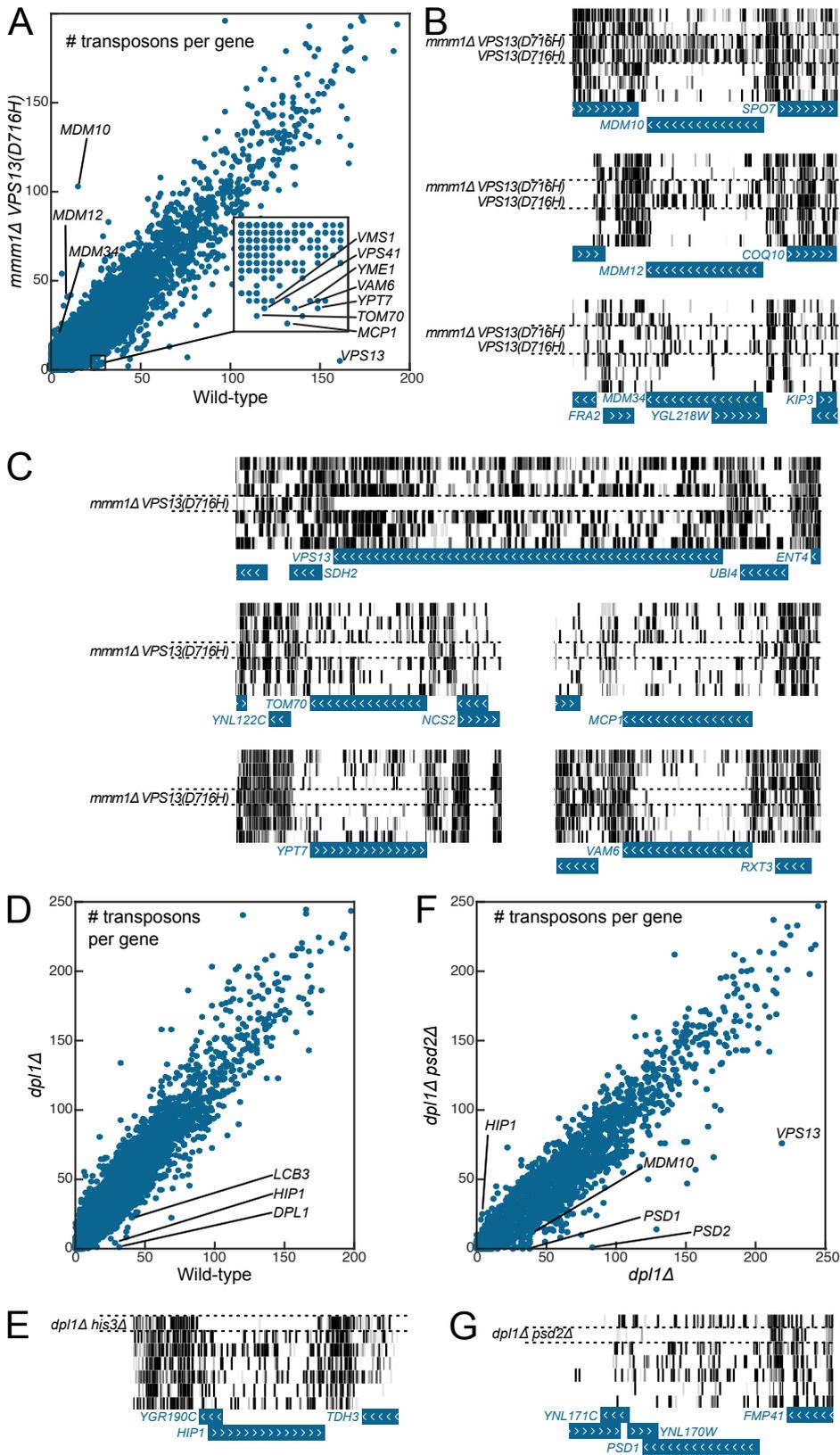
Figure 4 Supplement 1
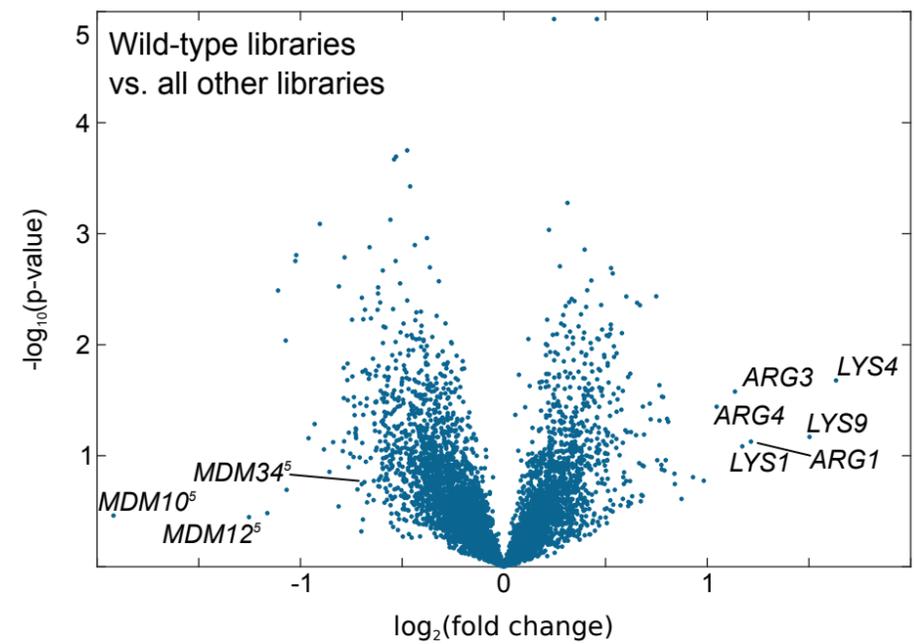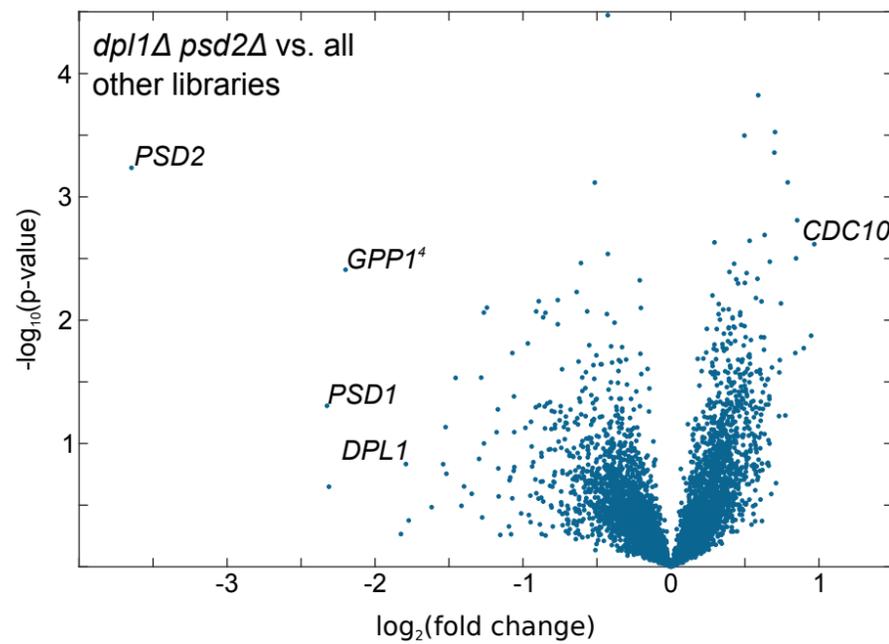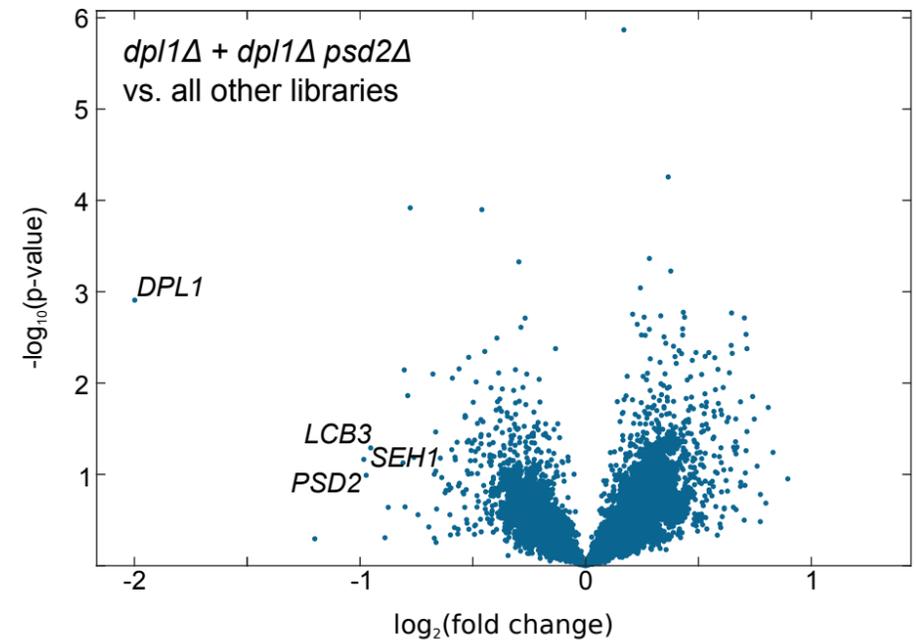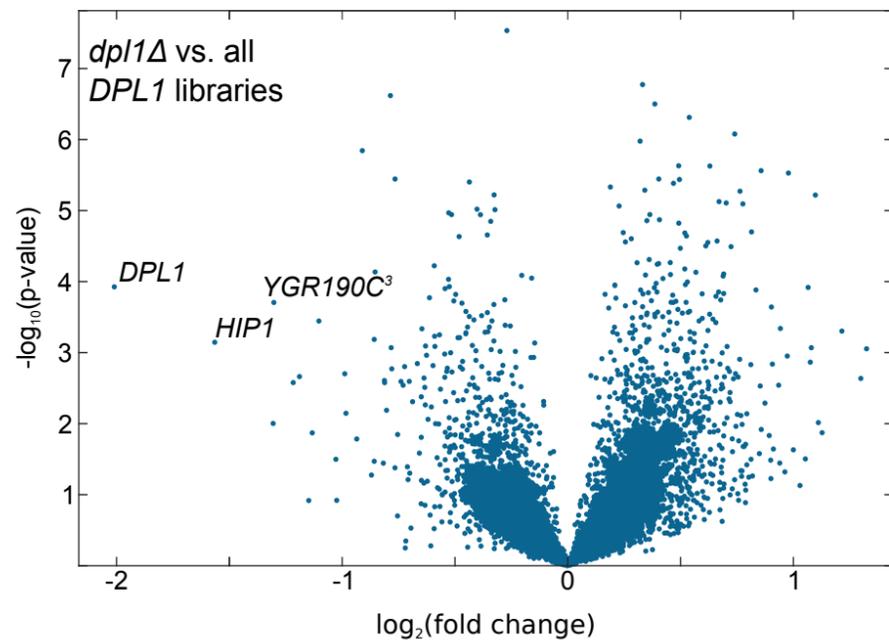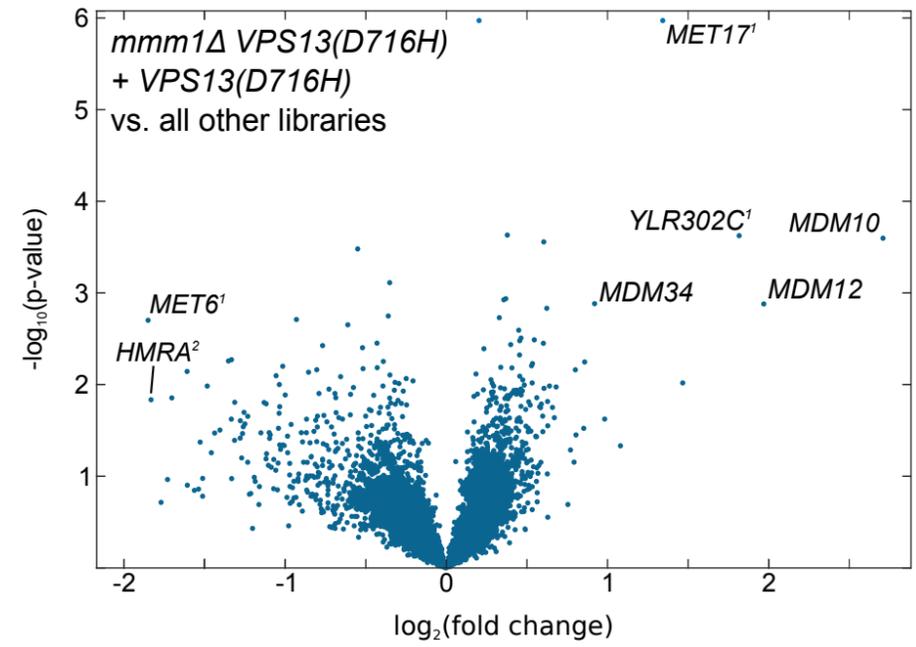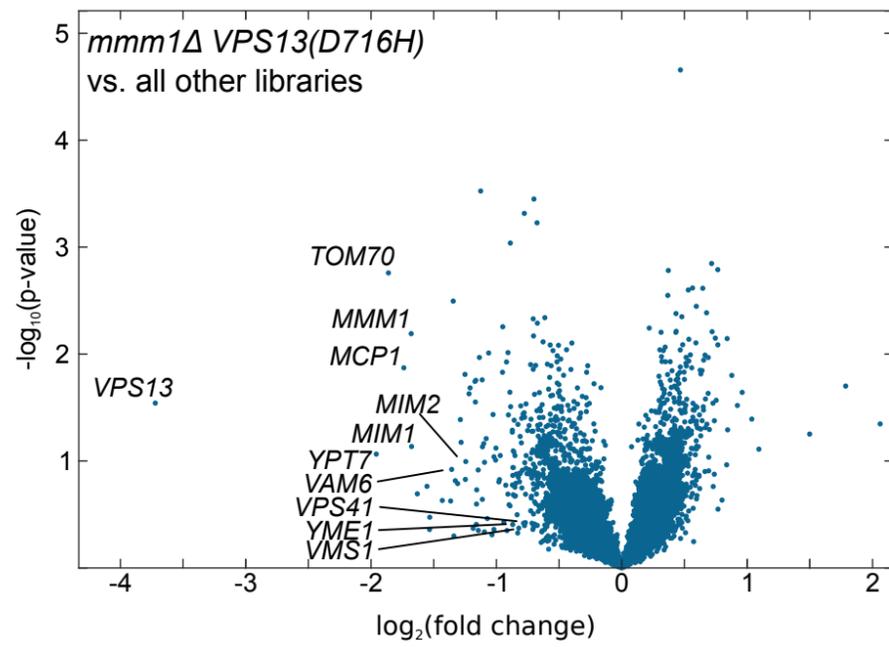
Figure 5
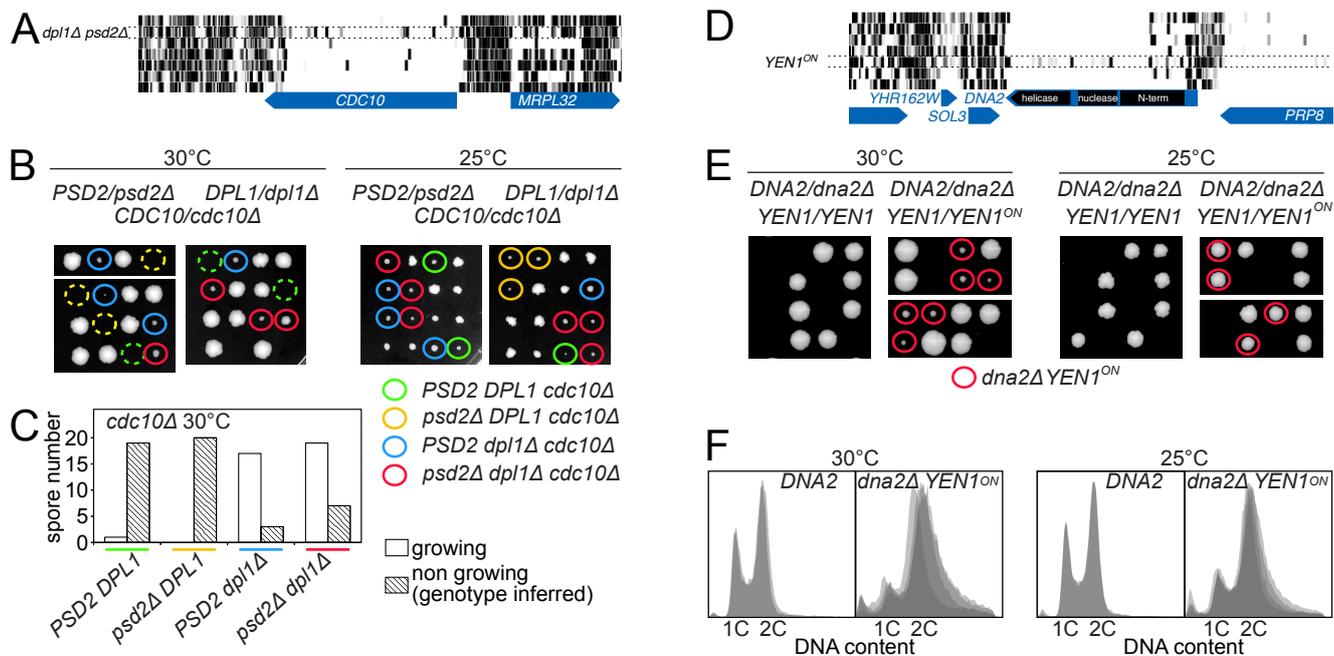
Figure 6

Figure 6 Supplement 1

A

B

C

D